

to appear in Chem. Soc. Rev. (2009)

Nanofluidics, from bulk to interfaces

Lydéric Bocquet* and Elisabeth Charlaix

*Laboratoire de Physique de la Matière Condensée et des Nanostructures; Université Lyon 1 and CNRS,
UMR 5586, 43 Bvd. du 11 Nov. 1918, 69622 Villeurbanne Cedex, France*

(Dated: October 22, 2018)

Nanofluidics has emerged recently in the footsteps of microfluidics, following the quest of scale reduction inherent to nanotechnologies. By definition, nanofluidics explores transport phenomena of fluids at the nanometer scales. Why is the nanometer scale specific? What fluid properties are probed at nanometric scales? In other words, why 'nanofluidics' deserves its own brand name? In this critical review, we will explore the vast manifold of length scales emerging for the fluid behavior at the nanoscales, as well as the associated mechanisms and corresponding applications. We will in particular explore the interplay between bulk and interface phenomena. The limit of validity of the continuum approaches will be discussed, as well as the numerous surface induced effects occurring at these scales, from hydrodynamic slippage to the various electro-kinetic phenomena originating from the couplings between hydrodynamics and electrostatics. An enlightening analogy between ion transport in nanochannels and transport in doped semi-conductors will be discussed.

I. NANOFLUIDICS, SURROUNDING THE FRAME

Nanofluidics, the study of fluidic transport at nanometer scales, has emerged quite recently in the footsteps of microfluidics. Pushing further the limits of fluidic downsizing is an attracting stream, in the spirit of scale reduction inherent to all micro- and nano- technologies. Various reasons may be seen as to motivate these novel developments. First, from the point of view of biotechnological ("lab on a chip") applications, decreasing the scales considerably increases the sensitivity of analytic techniques, with the ultimate goal of isolating and studying individual macromolecules [1, 2]. But also, from the point of view of fluidic operations, nanometric scales allow to develop new fluidic functionalities, taking explicit benefit of the predominance of surfaces. Typical examples involve preconcentration phenomena [3], the development of nanofluidic transistors [4, 5] or the recently proposed nano-fluidic diodes [6, 7]. But the analogy to micro-electronics is somewhat limited: fluid molecules are not electrons and the notion of large scale integration for fluidic devices, *i.e.* nanofluidics as a way of increasing the density of fluidic operations on a chip even further, is probably not a pertinent goal to reach for fluidic operations.

But from a different perspective, nanofluidics also carries the hope that new properties will emerge by taking benefit of the specific phenomena occurring at the smallest scales: new solutions may be obtained from the scales where the behavior of matter departs from the common expectations. The great efficiency of biological nanopores (in terms of permeability or selectivity) is definitely a great motivation to foster research in this direction [8, 9].

There is indeed a lot of room for improvements at these smallest scales: the example of aquaporins (AQP) is interesting in this context. Aquaporins channels are a key component of many biological processes [10] and play the role of water filters across biological membranes. These channels fulfill the conflicting tasks of being both extremely permeable to water, while extremely selective for other species [8]. To give an order of magnitude, the permeability of the water channel is typically *3 orders of magnitude larger* than what would be expected on the basis of the classical fluid framework for the same pore size [11, 12]. A potential answer is that AQP, although a filter for water, is mainly *hydrophobic*, *i.e.* water repellent! Of course some hydrophilic polar nodes are distributed along the pore, so as to keep water in the mainly hydrophobic environment. Quoting the terms of Sui *et al.* in Ref. [8], "*the availability of water-binding sites at these nodes reduces the energy barrier to water transport across this predominantly hydrophobic pathway, while the relatively low number of such sites keeps the degree of solute-pore interaction to a minimum. In balancing these opposing factors the aquaporins are able to transport water selectively while optimizing permeability.*" Beyond this elementary picture, understanding how AQP fulfills its challenging properties would definitely be a source of inspiration and open new perspectives for technological breakthrough in filtration, desalination, power conversion, ... However reproducing such a delicate composite (patched) architecture in bio-mimetic membranes is a great challenge, which requires breakthrough in the conception of its elementary constituents. But it points out that surfaces and their chemical engineering are a key actor to optimize fluid properties at nano-scale.

However, in its roots, nanofluidics is not a new field: as judiciously recalled by Eijkel and van den Berg in their pioneering review on the subject [1], many 'old' fields of physics, chemistry and biology already involves the behavior of fluids at the nanoscale. Like Monsieur Jourdain in "Le bourgeois gentilhomme" by Molière, one has done

*Electronic address: lyderic.bocquet@univ-lyon1.fr

'nanofluidics' for more than forty years without knowing it [151]. One may cite for example the domains of electro-kinetics (electro-osmosis or -phoresis, ...) with applications in chemistry and soil science, membrane science (ultra-filtration, reverse osmosis, fuel cells, ...), colloid chemistry, and of course physiology and the study of biological channels [1]. An interesting question is accordingly whether – on the basis of the novel 'nanofluidic' point of view – one may go beyond the traditional knowledge in those 'old' fields and obtain unforeseen results, *e.g.* allowing for better optimization of existing technologies? Our belief is that the answer to this question is already positive and this is one of the key aspects that we shall discuss in this review.

Finally it is also important to note that nanofluidics has emerged recently as a scientific field (*i.e.* naming a field as "nanofluidics") also because of the considerable progress made over the last two decades in developing nano-fabrication technologies, now allowing to fabricate specifically designed nanofluidic devices, as well as the great development of new instruments and tools which give the possibility to investigate fluid behavior at the nanometer scale. One may cite for example: new electrical detection techniques, Surface Force Apparatus (SFA), Atomic Force Microscopy (AFM), nano-Particle Image Velocimetry (nano-PIV) coupling PIV to TIRF set-up (Total Internal Reflection Fluorescence), as well as the considerable progress made in computational techniques, like Molecular Dynamics simulations. It is now possible to *control/design* what is occurring at these scales, and *observe/measure* its effects. This is the novelty of the field, and the reason why nanofluidics now deserves its own terminology.

The paper is organized as follows: In the second section we will replace nanofluidics in the perspective of the various length scales at play in fluid dynamics. We shall in particular discuss the limits of validity of continuum (*e.g.* hydrodynamic) descriptions. In the third section we discuss the dynamics of fluid at interfaces and the nanofluidic tools which have been developed recently to investigate it. In the fourth section we will explore various transport phenomena occurring in diffuse layers. In the fifth section we raise the question of thermal noise in nanofluidic transport. Finally we will conclude by exploring some general consideration and expectations about nanofluidics, especially in terms of energy conversion and desalination.

As a final remark, this review, like any review, is our subjective and personal view of the field of nanofluidics and the perspectives one may foresee. We organized our exploration around the length scales underlying fluid dynamics at the nanometric scales and how nanofluidics allows to probe the corresponding mechanisms. Accordingly, our aim is not to explore exhaustively the – already large – literature of the domain, but merely to disentangle the various effects and length scales underlying the behavior of fluids at the nanometer scales. In doing so, we certainly hope that this review will raise

new questions, open new directions and attract people in this fascinating domain.

II. LIMITS OF VALIDITY OF CONTINUUM DESCRIPTIONS AND NANOFUIDIC LENGTH SCALES

The introduction of the terminology "nanofluidics" (furthermore to define a specific scientific field) suggests that something special should occur for the transport of a fluid when it is confined in a channel of nanometric size. This leads to an immediate question: why should the nanometer length scale have anything specific for fluidic transport? Nanofluidics "probe" the properties of fluids at the nanoscale: so, what does one probe specifically in the nanometer range?

Actually one may separate two different origins for finite-size effects associated with nanometer scales: *bulk* and *surface* finite-size effects. The former, *bulk* effects are intimately associated with the question of validity of the classical continuum framework, in particular the Navier-Stokes equations of hydrodynamics: when do such descriptions breakdown? Can one then expect 'exotic' fluid effects associated with the molecular nature of the fluid? On the other hand, *surface* effects play an increasingly important role as the "surface to volume ratio" increases (*i.e.* as the confinement increases). We already pointed out the importance of such effects on the example of AQP water channels. As we show below, the surface effects occur at much larger scales than the 'bulk' deviations from continuum expectations.

The discussion on the length scales at play, to be explored in this section, is summarized in Fig. 1.

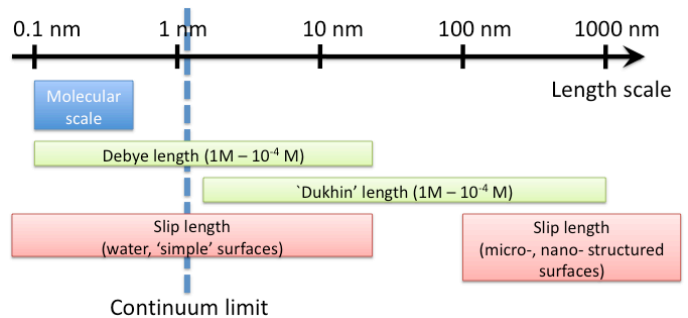


FIG. 1: Various length scales at play in nanofluidics.

A. Validity of bulk hydrodynamics

We first start with a short discussion on the validity of bulk hydrodynamics. In practice, this raises the question: when do the Navier-Stokes (NS) equations breakdown? These equations were developed in the 19th century to describe fluid flows at, say, the human scale. What comes

as a surprise is their incredible robustness when applied to ever smaller scales.

As a fact, for simple liquids, **the continuum framework of hydrodynamics is apparently valid down to the nanometer scale.** In other words, there is no expected deviations to the bulk NS equations for confinement larger than $\sim 1\text{nm}$. This very surprising result is actually suggested by a number of experimental and molecular simulations studies. On the experimental side, one may cite the early work by Chan and Horn [13] and later by Georges *et al.* [14] using Surface Force Apparatus, where the prediction of hydrodynamics (the Reynolds formula in their case) was verified to be valid for confinement larger than typically ten molecular diameters. More recently, and specifically for water, the works by Klein *et al.* [15] and E. Riedo *et al.* [16] showed that water keeps its bulk viscosity down to $\sim 1 - 2\text{nm}$, with a drastic change of behavior for stronger confinements, where the wettability of the confining surface plays a role [16]. A similar behavior was found for other liquids like octamethylcyclotetrasiloxane (OMCTS) [17, 18].

This threshold for the applicability of continuum hydrodynamics was also investigated using Molecular Dynamics simulations of confined water, and the same value of about 1 nm came out of the simulation results [19, 20, 21]. Furthermore, it is interesting to note that beyond the validity of continuum equations, the value of the viscosity also remains quantitatively equal to its bulk value. We show in Fig.2 the results of MD simulations for the viscosity η of water (SPC-E model) measured in various confinements. The value of the viscosity is obtained by measuring the shear-stress on the confining plates for a given shear-rate (corrected for slippage effects). As shown on this figure, the shear viscosity of water keeps its bulk value down to confinements of $\approx 1\text{nm}$ (typically 3 water layers).

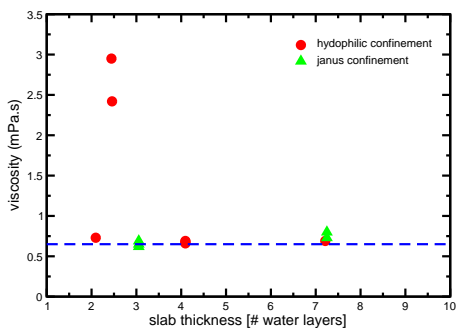


FIG. 2: Viscosity of water versus confinement, as measured from MD simulations of water confined in a nano-slit made of either two hydrophilic walls, or one hydrophilic and one hydrophobic wall (janus confinement). [courtesy of D. Huang]

Now, in contrast to the viscosity, other transport co-

efficients may be more strongly affected by confinement. This is the case for example of the (self-)diffusion coefficient which was shown to depend algebraically on the confinement width [22, 23]. As a consequence, the diffusion coefficient in confinement strongly departs from its Stokes-Einstein prediction, $D = k_B T / (3\pi\eta\sigma)$, with σ the molecule diameter. The latter is accordingly not a correct measure of the viscosity, as sometimes assumed [19, 24].

Fundamentally the validity of NS equations down to typically 1nm (for water) is *a priori* unexpected. Navier-Stokes (NS) equations have been developed to account for the fluid dynamics at 'large' scales and they rely on an assumption of a local and linear relationship between stress and velocity gradients.

To our knowledge, there is no firmly grounded argument for this validity and we propose here a few tentative leads. NS equations, like any continuum framework, rely actually on the key assumption of a separation of length- and time- scales between the investigated length scale and the 'molecular' dynamics. This is the "hydrodynamic limit", in which the continuum framework should hold. Under this time- and length- scale separation, the microscopic dynamics associated with a huge number of degrees of freedom $\mathcal{N} \approx 10^{23}$ reduces to equations with just a few degrees of freedom (velocity field, pressure, density, temperature, etc.), while all the complexity is hidden in just a few phenomenological coefficients. Achieving this averaging out of the "fast variables" is a huge challenge which can be achieved systematically only in a few limiting cases, see *e.g.* [25] for an explicit example. In general, the elimination of fast variables is summarized in the Green-Kubo relationship for the transport coefficients: for example the shear viscosity η can be expressed as the integral of the stress-stress correlation function according to

$$\eta = \frac{1}{Vk_B T} \int_0^\infty \langle \sigma_{xy}(t) \sigma_{xy}(0) \rangle_{\text{equ}} dt \quad (1)$$

with σ_{xy} a non diagonal component of the stress tensor [26] and $\langle \cdot \rangle_{\text{equ}}$ denotes an equilibrium average.

The time-scale separation underlying the validity of Eq. (1) requires the microscopic time scales, τ_σ , characterizing the stress-stress correlation function, to be much smaller than a hydrodynamic time scale. This time scale is *e.g.* the relaxation time of momentum, which for a given wave vector q has the expression $\tau_q = (\nu q^2)^{-1}$, with $\nu = \eta/\rho$ the kinematic viscosity and ρ the mass density. An implicit condition of validity is accordingly $\nu q^2 \tau_\sigma < 1$. This fixes the limit for time-scale separation at confinements w larger than a viscous length scale:

$$w > \ell_c = \sqrt{\nu \cdot \tau_\sigma} \quad (2)$$

Putting numbers for water, a typical correlation time for the stress-stress correlation function is in the picosecond range $\tau_\sigma \sim 10^{-12}\text{s}$, while $\nu = 10^{-6} \text{m}^2 \cdot \text{s}^{-1}$. Altogether this gives for water

$$\ell_c \approx 1\text{nm} \quad (3)$$

A nanometric characteristic length scale thus emerges naturally as a lower bound for the validity of the notion of viscosity, and thus for the application of standard NS hydrodynamics. This is indeed the experimental value below which strong departure from the continuum framework is observed.

Of course, it would be interesting to explore further the physical contents of this condition: what occurs for smaller confinements? Also, can one tune ℓ_c in specific systems? etc.

In the extreme limit of single file transport, the transport behavior is indeed expected to strongly deviate from the bulk expectations, with the predicted occurrence of anomalous diffusion, and a fast stochastic transport, to cite some examples [28, 29, 30]. Apart from biological systems –where molecular pores are the rule–, fabricating channels with molecular size is however still out of reach with state-of-the-art nanofabrication technologies.

As a side remark, it would be interesting to extend this discussion to other transport phenomena, like for example heat transfer at nanoscales. Heat transfer from nanoparticles and nanostructures to a fluid is an actively growing field, *e.g.* in the context of cooling enhancement by structured surfaces or local heating of fluids via nanoparticles [27]. Similar arguments as above may be proposed, and lead to an equivalent sub-nanometer heat length scale (for water at room temperature). This suggests that the continuum phenomenological picture for heat transport in fluids, involving Fourier law, is expected to hold down to nanoscales, in agreement with observations [27]. However a full investigation of the limit of applicability of the corresponding continuum phenomenological laws remain to be developed in general.

A conclusion of the above discussion is anyway that for most nanofluidic applications involving water in suprananometric confinements, bulk NS equations can be safely used to account for the fluid transport.

B. A broad spectrum of length scales

Aside from ℓ_c introduced above, there is a number of length scales which enter nanofluidic transport. These length scales are all related to surface effects in one way or another. We review in this section a panel of these length scales, climbing up from the smallest – molecular – scales to the largest, but still nanometric, scales. This panel is not exhaustive, and we merely insist on the main length scales which appear generically in nanofluidic problems. Our aim is to show that there are a number of pertinent scales which lie indeed in the nanometric range. This implies that specific nanofluidic phenomena will show up when the confinement compares with these values.

1. Molecular length scales

At the smallest scales, the granularity of the fluid and its components (solvent, ions, dissolved species, ...) should play a role. This is defined by the molecular scale, associated with the diameter of the molecules σ , typically in the angström scale, 3\AA for water. As we discussed above, this is the scale where the validity of hydrodynamics breaks down, typically for confinements of 3-5 molecular diameter. Various phenomena then come into play. First, the structuration and ordering of the fluid at the confining walls plays a role. Such ordering was indeed shown experimentally to induce oscillatory dissipation in liquid films with a width of several molecular diameter [17, 18].

Similarly non-local rheological properties have been predicted in strongly confined situations [31], associated with a length characterizing non-locality typically in a few diameters range (indeed in line with the above limit of NS hydrodynamics). This result echoes recent findings of non-local flow curves in confined soft glasses [32]. An interesting consequence of non-locality, as pointed out in [32], is that the specific nature of surfaces does influence the global flow behavior in confinement, in line with recent observations in AFM measurements by Riedo *et al.* for strongly confined water (less than 1nm) films at a hydrophilic and hydrophobic surfaces [16].

But even more drastic are the deviations occurring in the extreme limit where only one molecule can enter the confining pore. Very strong correlations and collective motion builds up in the liquid dynamics, leading to the so-called “single-file” transport [33, 34]. The associated transport differs strongly from the bulk hydrodynamic predictions and various specific phenomena show up, like non-fickian transport [34], fast water transport and ion transfer, stochastic flow with the occurrence of “bursts”, etc., see *e.g.* [33]. Simulations of water transport through single-file carbon nanotubes (where only one water molecular can pass through the channel) showed indeed flow rate much larger than those predicted from the Poiseuille law of hydrodynamics [28].

Note however that this behavior is limited to nanochannels where molecules cannot cross each other, *i.e.* with diameters not exceeding the water molecular length scale, like in biological channels. Up to now, artificially produced nanochannels do not reach this limit. This point is interesting to discuss in the context of recent experimental results obtained for flow through carbon nanotube membrane [9, 35, 36]. A recent experimental first was achieved in the group of O. Bakajin, who investigated the flow through a membrane constituted of carbon nanotube with a size in the range 1.3-2 nm [9], following the work on larger nanotubes ($\sim 7\text{nm}$) by Majumder *et al.* [35]. These works demonstrated massively enhanced flow permeability, as compared to bulk predictions (in term of slippage, to be discussed below, this would correspond to slip lengths up the micron, far above any expected result for these surfaces). More

recent experiments performed with membranes made of wider carbon nanotubes suggest a large, but still smaller, enhancement of the permeability [36]. Therefore, while it would be tempting to discuss these results in the context of single-file transport and the predictions by Hummer *et al.* on fast single-file transport in sub-nanometer carbon nanotube [33], this point of view is difficult to justify: as discussed above, fluid flow in nanotube pipes with a supra-nanometric diameter can be safely described by continuum approaches (Stokes equation) and the dynamics is definitely not single file. Molecular Dynamics simulations of flow through similar carbon nanopipes indeed suggest large flow enhancement [24, 37], but still far below the experimental results. There is therefore a strong need to perform flow experiments through a single object, *i.e.* through a single carbon nanotube. This is still an experimental challenge.

Altogether transport at the molecular scale offers a rich panel of transport behavior. This is definitely the scale where, as we quoted in the introduction, new solutions and technological breakthrough could emerge as the behavior of matter departs from the common expectations. This suggests that the molecular scale would be the ultimate scale to reach for nanofluidics. But at present, producing channels of sub-nanometric size remains a technological challenge.

2. Electrostatic length scales and their dynamic influence

The scales associated with the interaction of the flowing matter with its environment also enter the game. And of course, electrostatic plays a key role in this context. We leave aside interactions deriving indirectly from electrostatics to focus on the interactions between charged species. These obviously concern ions dissolved in the fluid: ion-ion interaction, and interactions of ions with charged surfaces. This also involves the dipolar interaction among water molecules, as well as H-bonding.

Electrostatics involves a rich panel of length scales. And more importantly, due to the long range nature of electrostatics, these length scales are intimately coupled: effects occurring at the smallest electrostatic lengths do climb the scales to span the whole range.

a. Bjerrum length (and some derivatives)

We start with the Bjerrum length, ℓ_B , which is defined as the distance at which the electrostatic interaction \mathcal{V}_{el} between two charged species becomes of the order of the thermal energy, $k_B T$: $\mathcal{V}_{el}(\ell_B) \approx k_B T$. For two ions, with valence z , embedded in a dielectric medium with dielectric constant ϵ , this takes the form

$$\ell_B = \frac{z^2 e^2}{4\pi\epsilon k_B T} \quad (4)$$

(e the elementary charge). For bulk water at ambient temperature and a valency $z = 1$, this gives $\ell_B = 0.7\text{nm}$.

The Bjerrum length therefore compares with the molecular range in this case. Note however that for multi-valent ions or for organic solvent with lower dielectric constants, ℓ_B may be much larger and thus separate from the molecular range.

Other length scales could be introduced along the same lines by comparing thermal energy to *e.g.* charge-dipole, dipole-dipole, etc. interactions, taking into account the multi-pole interaction under consideration. This leads *a priori* to length scales smaller than the Bjerrum length introduced above. For the charge-dipole interaction, this gives for example $\ell_d = (\ell_B p_e^2)^{1/2}$, with p the dipole strength: for water parameters, ℓ_d is in the Angström range. It does correspond to the typical thickness of a hydration layer around an ion [38].

By definition, the Bjerrum length (and its derivatives like ℓ_d above) is the scale below which direct electrostatic interactions dominate over thermal effects. Its consequences on nanofluidic transport is thus expected at molecular scale. For example, for confinement below ℓ_B one expects a large free-energy cost to undress an ion from its hydration layer and make it enter a molecular pore. This has therefore immediate consequences on the filtering process of charged species, as in biological ion channels.

But as pointed out above, a strong interplay with upper scales is expected due to the long range nature of electrostatic interactions. For example, as we will discuss in section IV, ion-specific effects at interfaces, the origin of which occurs at a scale ℓ_B , have strong effects on the electro-kinetics at nanometric, micrometric and even larger scales.

b. Debye length scale

A central concept of electrostatics is the notion of electrostatic diffuse layer (EDL). At a charged interface, the EDL is the region where the surface charge is balanced by the cloud of counterions. In this region the ion concentration profiles depart from their bulk values due to the interaction of ions with the surface charge. This is therefore the region where local electro-neutrality is not obeyed.

The Debye length emerges naturally from the Poisson-Boltzmann theory and characterizes the electrostatic screening in the bulk electrolyte [39]. It is defined in terms of the salt concentration ρ_s according to the expression:

$$\lambda_D = (8\pi\ell_B\rho_s)^{-1/2} \quad (5)$$

Note that in this expression, as in the following, ρ_s denote the salt concentration *in the reservoirs*, thereby fixed by the chemical potential of the ions. The value of the Debye length depends on the salt concentration and ranges typically between tens of nanometer (30 nm for $\rho_s = 10^{-4}\text{M}$) down to Angströms (3 Å for $\rho_s = 1\text{M}$). In physical terms, the electrostatic free-energy of an ion

ressed by its spherical cloud of counterions with size λ_D is of the order $k_B T$.

The Debye length characterizes the width of the EDL. Interestingly, it is independent of the surface charge and only depend on the bulk ion concentration. However, in the limiting case of a salt free solution (with $\lambda_D \rightarrow \infty$), the width of the diffuse layer is merely fixed by the so-called Gouy-Chapman length, to be defined in the next paragraph.

The Debye length plays a central role in nanofluidics for various reasons. First, as quoted above, this is the region in the fluid close to charged surfaces where local charge electroneutrality is broken. Under an applied electric field, this is thus the region where volume electric forces, $f_e = \rho_e E_e$, will apply, with ρ_e the charge density and E_e an applied electric field. On the other hand these forces vanish in the bulk of the material due to a vanishing charge density $\rho_e \rightarrow 0$ far from the surfaces. Therefore tuning the fluid properties inside the nanometric EDL is expected to affect the whole response of the system under an electric field. Accordingly, tuning the dynamics of the fluid in the nanometric EDL, or modifying its structure, will have a macroscopic impact on the fluid dynamics at scales much larger than the Debye length. We will come back extensively on this question below, in section IV B.

Second, a specific behavior is expected when the Debye layers overlap in a nanopore, which occurs when its size is of the order of twice the Debye length. This phenomenon has a strong effect on fluidic transport and has been the object of intense research recently, as reviewed recently by Schoch *et al.* [40], see Sec. IV. One may cite in particular the phenomena of ion enrichment and exclusion [2]. While these phenomena were known for a long while in membrane technology, they found new applications in the field of nanofluidics. It is at the root of a number of novel fluidic phenomena, such as permselectivity [2], nanofluidic diodes [6, 7] or surface dominated ion transport [41].

A key practical aspect is that the condition of Debye layer overlap is much less stringent to fulfill with actual nanofabrication techniques. These are now able to produce individual nanopores with at least one dimension in the range of ten nanometers, *i.e.* potentially suited for Debye layer overlap.

c. Length scales associated with surface charge: Gouy-Chapman and Dukhin

Other electrostatic length scales may be constructed on the basis of surface electrostatic properties. We already mentioned the *Gouy-Chapman length scale*, which shows up for the behavior of a salt solution very close to a charged surface. For a surface charge density Σe , this has an expression $\ell_{GC} = 1/(2\pi\Sigma\ell_B)$. In contrast to the Debye length, the Gouy-Chapman length depends explicitly on the surface density Σ of charges of the confining surface (Σ in units of m^{-2}), but not on the bulk ion con-

centration. Physically, the Gouy-Chapman length can be defined as the distance from the wall where the electrostatic interaction of a single ion with the wall becomes of the order of the thermal energy. For typical surface charges, say $\Sigma e \sim 50 \text{ mC/m}^2$ ($\approx 0.3 e/\text{nm}^2$) to fix ideas, then $\ell_{GC} \sim 1\text{nm}$. The Gouy-Chapman length plays a role for solutions with very small salt concentration. This has an influence on the conductance in nanochannels as we discuss in Sec. IV C.

More interesting is a length which can be defined on the basis of the comparison between the bulk to the surface electric conductance (relating electric current to an applied electric field). This introduces what can be termed as a ‘‘Dukhin length’’, by analogy to the Dukhin number usually introduced for colloids [152]. Indeed the conduction probes the number of free carriers (ions), so that in a channel of width h and surface charge Σ , the equivalent bulk concentration of counterions is $2\Sigma/h$. One may define a Dukhin number $Du = |\Sigma|/(h\rho_s)$, where ρ_s is the concentration of the salt reservoir [42]. A ‘Dukhin length’ can then be defined as

$$\ell_{Du} = \frac{|\Sigma|}{\rho_s}. \quad (6)$$

To put numbers, for a surface with a surface charge density $e\Sigma \sim 50\text{mC/m}^2$ ($\approx 0.3e/\text{nm}^2$), ℓ_{Du} is typically 0.5 nm for $\rho_s = 1\text{M}$, while $\ell_{Du} = 5 \mu\text{m}$ for $\rho_s = 10^{-4}\text{M}$! The Dukhin length characterizes the channel scale below which surface conduction dominates over the bulk one. In a different context of charge discontinuities at surfaces, it has also been interpreted in terms of an electrokinetic ‘‘healing’’ length [43].

This length scale can actually be rewritten in terms of the Debye and Gouy-Chapman lengths as $\ell_{Du} \sim \lambda_D^2/\ell_{GC}$. Note also that in the limit where the Debye length is large compared to the Gouy-Chapman length, $\ell_{GC} < \lambda_D$, the non-linear Poisson-Boltzmann expression for the electrostatic potential [39] allows to rewrite the above length as $\ell_{Du} \sim \lambda_D \exp[e|V_s|/2k_B T]$, with V_s the surface potential. The corresponding form for the Dukhin number is more standard in colloid science [42].

This length plays an important role for the conductance in nanochannels, cf Sec. IV C, where surface effects are shown to strongly affect conductance [41, 44].

3. Slip lengths and surface friction

Up to now we merely considered length scales characterizing the structure of the fluid and its components (ions, ...). However the *dynamics* of fluids at interfaces introduce various length scales. This is in particular the case of the so-called *slip length*, b , characterizing the hydrodynamic boundary condition of a fluid at its confining interfaces. The latter is defined according to the Navier boundary condition (BC) as [21]

$$b \partial_n v_t = v_t \quad (7)$$

with n, t points to the normal and tangential directions of the surface, v_t is the tangential velocity field and b the slip length. The slip length characterizes the friction of the fluid at the interface and large slip lengths are associated with low liquid-solid friction.

This point has been amply explored experimentally and theoretically: a key result which emerges from this measurements is that the slip length of water at solid surfaces depends crucially on the wettability of the surface [21, 45]. We will come back more exhaustively on this point in Sec. III. At this level, one should keep in mind that slip lengths in the range of a few ten nanometers are typically measured on hydrophobic surfaces, while b is sub-nanometric on hydrophilic surfaces. Note however that very large slip length, in the micron range, may be obtained on nano- and micro- structured interfaces [46, 47].

This offers the possibility to modify the nanofluidics in pores using chemical engineering of the surfaces. As the pore size compares with b a considerable enhancement of fluid transport is accordingly expected. Furthermore one may remark that these values of b also compares with typical Debye lengths. Therefore slippage effects are expected to affect ion transport at charged surfaces. We will discuss these aspects more exhaustively below.

A final remark is that other surface related lengths may be constructed. This is the case in particular of the Kapitza length, which characterizes the boundary condition for thermal transport across an interface, see *e.g.* [21]. The Kapitza length behaves quite similarly to the slip length and strongly depends on the wettability of the interface [48].

4. Other length scales

The review of length scales above is not exhaustive and many other length scales may enter the game, depending on the problem, geometry and system considered. For example, in the context of transport of macromolecules (colloids, polymers, DNA, RNA, proteins, ...), the typical size of the particle – diameter or radius or gyration – plays of course a central role. More precisely a key quantity is the free energy associated with the confinement of the macromolecule, \mathcal{F}_c which fixes the partitioning of the molecule in the nanopore w.r.t. the bulk. The probability of passage of a macromolecule through a pore is expected to scale like $\exp[-\mathcal{F}_c/k_B T]$, hence fixing its permeability [49]. For example for a polymer chain confined in a pore with size D , the entropic cost of confinement takes the form $\mathcal{F}_c \approx k_B T (R_g/D)^{1/\nu}$, with $R_g = a \times N^\nu$ the radius of gyration of the polymer (a the monomer size and N the polymer length). For a polymer in good solution, the Flory exponent is $\nu = 5/3$. Pores the size of which is below the radius of gyration of the molecule thus act as molecular sieve. This has been explored in various experiments of polymer translocation in nanopore following the pioneering work of Bezrukov *et al.* [50, 51] and

Kasianowicz[52], as well as in the context of DNA separation [53].

C. Some practical conclusions

The discussion above is summarized in Fig.1, where we organized the various scales at play along the scale axis. This points to several conclusions.

1. A number of specific phenomena occur in the nanometric range, which indeed justifies the specificity of the dynamics of fluids in the nanometer range, *i.e.* nanofluidics.
2. An important conclusion is : For water under normal conditions, the Navier-Stokes equation remains valid in nano-channels down to typically 1-2 nanometers. This is good and bad news. Good because *one may safely use NS equations for most nanofluidic phenomena*. This robustness of continuum hydrodynamics is remarkable.

But this is in some sense *bad news* since it means that reaching specific effects associated with the granularity of the fluid requires molecular confinement, *i.e.* confinement below the nanometer. Producing nanochannels with such sizes is technologically difficult to achieve. On the other hand, this probably explains why most biological channels have a molecular entanglement: to reach specificity and avoid the “universality” associated with continuum equations, one should reach the fluid molecular scale.
3. This suggests that the molecular pore is the ultimate scale to reach for nanofluidics, where, as we quoted in the introduction, new solutions and technological breakthrough could emerge as the behavior of matter departs from the common expectations. But at present, there is however still a long way before this scale is technologically accessible.
4. While it remains difficult to tune the bulk behavior of the confined fluid, there are much more room and possibilities to benefit from surface effects. This is clearly apparent in Fig. 1, where surface effects enter the nanofluidic game at much larger length scales. Surface effects enter in particular via the Debye length, Dukhin length, slip length, all typically in ten nanometers range (and even more for the Dukhin length). This suggests that specific effects will show up when one of these lengths will compare with the pore width. Furthermore, particular effects should also occur when two of these lengths become comparable, independently of the confinement. This will be explored in Sec. IV.

Altogether nanofluidics is a incredible playground to play with surface effects !

III. DYNAMICS AT SURFACES AND THE TOOLBOX OF NANOFUIDICS

We have discussed above that the bulk laws of hydrodynamics are valid down to very small scales, typically $\sim 1\text{nm}$, so that bulk Navier-Stokes equations can be used for most nanofluidic flows. However as the size of the nanochannel decreases, the dynamics at its surface should play an increasingly important role. Navier-Stokes equations require boundary conditions (BC) for the hydrodynamic flow at the device's surface, and a specific knowledge of these BC is a pre-requisite to apprehend flow at the nanoscale.

As we quoted above, the BC at a solid surface introduces a new length, the so-called Navier length or slip length, which relates the tangential velocity v_t to the shear rate at the wall [54]:

$$v_t = b \frac{\partial v_t}{\partial z} \quad (8)$$

Obviously the control of the slip length is of major importance for flows in confined geometries, and it can have dramatic consequences on the pressure drop, electrical, and diffusive transport through nanochannels. For instance the relative increase in hydraulic conductance of a cylinder of radius r due to wall slippage is $1 + 6b/r$; it can be much larger for the electrical conductance or electro-osmosis, as we will discuss in the sections below.

As a consequence a sustained interest has been devoted in the last ten years for the investigation of the BC and its dependence on interfacial properties, such as the surface topography and the liquid-solid interactions. Reviews on this subject are [21, 55, 56].

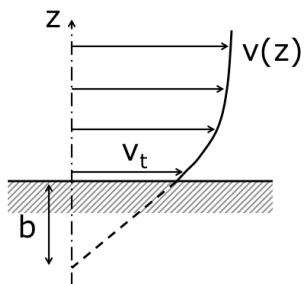


FIG. 3: Hydrodynamic slip and definition of the slip length b : the slip length is the distance in the solid at which the linear extrapolation of the velocity profile vanishes.

A. Theoretical expectations for slippage

The theoretical understanding of slippage has been the object of intense research over the last decade, see Ref. [21] for a review. The BC has been studied theoretically by Molecular Dynamics simulations, as well as in the context of linear response theory [45, 57, 58, 59, 60, 61, 63].

It is now well understood that the BC on atomically smooth surfaces depends essentially on the structure of the liquid at the interface, itself determined by its interactions, its commensurability with the solid phase, and its global density [21].

In order to connect the slip length to the interfacial properties, it is useful to interpret the slip length in terms of liquid-solid friction at the interface. The friction force at the liquid-solid interface is linear in slip velocity v_t :

$$F_f = -\mathcal{A} \lambda v_t \quad (9)$$

with λ the liquid-solid friction coefficient and \mathcal{A} the lateral area. By definition the slip length is related to the friction coefficient according to $b = \eta/\lambda$, with η the bulk viscosity. As a phenomenological friction coefficient, λ can be expressed in terms of equilibrium properties in the form of a Green-Kubo (GK) relationship [21, 59, 62]:

$$\lambda = \frac{1}{\mathcal{A} k_B T} \int_0^\infty \langle F_f(t) \cdot F_f(0) \rangle_{\text{equ}} dt \quad (10)$$

where F_f is the total (microscopic) lateral force acting on the surface. In practice, this expression is difficult to estimate. However some useful information on the slip length may be extracted from it.

A rough estimate of slippage effects can be proposed [63]. One may indeed approximate the GK expression as $\lambda \approx \frac{1}{\mathcal{A} k_B T} \langle F_f^2 \rangle_{\text{equ}} \times \tau$, with τ a typical relaxation time and $\langle F_f^2 \rangle_{\text{equ}}$ the mean-squared lateral surface force. We then write $\tau \sim \sigma^2/D$ where σ is a microscopic characteristic length scale and D the fluid diffusion coefficient, while the rms force is estimated as $\langle F_f^2 \rangle_{\text{equ}} \sim C_\perp \rho \sigma (\epsilon/\sigma)^2$, with ϵ a typical fluid-solid molecular energy, ρ the fluid density and C_\perp a geometric factor that accounts for roughness effects at the *atomic level* (large C_\perp corresponding to a larger atomic roughness) [45, 63]. Altogether this provides a microscopic estimate for the slip length as

$$b \sim \frac{k_B T \eta D}{C_\perp \rho \sigma \epsilon^2} \quad (11)$$

A more systematic derivation leads to a very similar result [21, 62], with Eq.(11) multiplied by the inverse of the structure factor of the fluid, $S_w(q_\parallel)$, computed at a characteristic wave-vector of the solid surface q_\parallel : $b \propto S_w(q_\parallel)^{-1}$. This term measures a kind of commensurability of the fluid with the underlying solid structure, in full analogy with solid-on-solid friction. Note also that the slip length depends on the product $\eta \times D$, so that according to the Stokes-Einstein relationship, the slip length is not expected to depend on the bulk fluid viscosity (except for specific situations where these two quantities can be decorrelated). The scalings proposed by the above simple estimate are in good agreement with molecular dynamics results [21, 63].

According to Eq.(11) significant slippage should occur on very smooth surfaces, in case of a low density

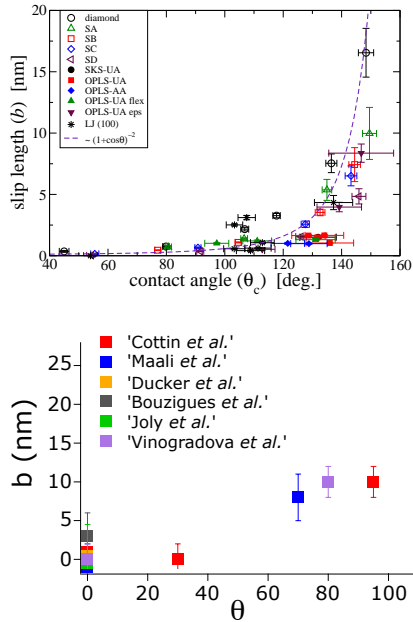


FIG. 4: Slip length b of water as a function of the contact angle on various smooth surfaces. *Top*: Results from Molecular Dynamics simulations by Huang *et al.* for the slip length of water on various surfaces, from Ref. [45]. The dashed line is a theoretical fit scaling like $b \propto (1 + \cos \theta)^{-2}$. *Bottom*: Compilation of various experimental results.

at wall - which requires both a moderate pressure and unfavorable liquid-solid interactions -, or a low value of $S_w(q_{\parallel})$, which characterizes liquid/solid commensurability. It also suggests that low energy surfaces, *i.e.* with small liquid-solid interaction ϵ , should exhibit large slippage. Accordingly, hydrophobic surfaces should exhibit larger slip length than hydrophilic ones.

We plot in Fig. 4 (top) results for the slip length obtained by Molecular Dynamics of a water model over a broad variety of surfaces [45, 63]. A 'quasi-universal' dependence of the slip length on the contact angle is measured, with - as expected from the above arguments - an increase of the slip length for more hydrophobic surfaces.

B. Experimental results

On the experimental side a race has engaged toward the quantitative characterization of BCs within the nanometer resolution, using the most recent developments in optics and scanning probe techniques [55, 56]. This experimental challenge has generated considerable progress in the experimental tools for nanofluidic measurements, and the values of the slip lengths reported had a tendency to decrease as the resolution and robustness of the techniques has increased. An intrinsic difficulty stems from the fact that the BC is a continuous

medium concept involving an hydrodynamic velocity averaged on many molecules in the liquid and extrapolated to the wall: it does not simply reduce to the velocity close to the surface of molecules or tracer particules, which are furthermore submitted to brownian motion and reversible adsorption. Also, the surface has to be smooth and homogeneous on the scale of the probed area in order to characterize an *intrinsic* BC, and not an *effective* slip length. Thus, the problem of the BC has been a discriminating test of the capacity of instruments to perform quantitative mechanical measurements at the nanoscale. We propose here a brief overview of the current state-of-the-art. This offers the opportunity to quote the various tools which have been developed recently to study flow and fluid dynamics at the nanofluidic scales.

The Surface Force Apparatus provided the first sub-nanometer resolution measurement of BCs, based on the viscous force F_v acting between two crossed cylinders whose distance D is measured within the Angstrom resolution by the so-called FECO interferometric fringes [64]:

$$F_v = \frac{6\pi\eta R^2 \dot{D}}{D} f_s^* \quad (12)$$

$$f_s^*(D/b) = \frac{D}{3b} \left[\left(1 + \frac{D}{6b}\right) \ln\left(1 + \frac{6b}{D}\right) - 1 \right] \quad (13)$$

with η the liquid viscosity and R the cylinder radius [65]. In case of a no-slip BC, F_v reduces to the Reynolds force between a sphere and a plane. Chan and Horn [13] investigated the flow of various organic liquids confined between atomically flat mica surfaces and showed that they obeyed the no-slip BC, with the no-slip plane located about one molecular size inside the liquid phase. Their results were confirmed by other experiments running the SFA in a dynamic mode, and extended to water and to various (wetting) surfaces [14, 66]. Further investigations focused on non-wetting surfaces and reported the existence of very large slip lengths ($\simeq 1\mu m$) associated to a complex behaviour, with slippage appearing only under confinement and above a critical shear stress [67]. However it was shown that elasto-hydrodynamics effects due to non perfectly rigid surfaces (such as glued mica thin films) retrieve this typical behaviour [68]. Experiments on rigid surfaces later reported the existence of substantial slippage of water on smooth homogeneous non-wetting surfaces, with a slip length increasing with the contact angle and reaching a range of 20nm at contact angles of 110° [69, 70], see Fig. 4.

The AFM with a colloidal probe operates along a similar principle but with a smaller probed area than the SFA. In pioneering investigations Craig *et al.* found a shear-rate dependent BC of sucrose solutions on partially wetting SAMs, with slip lengths reaching 20nm at high velocities [71], while Bonacurso *et al.* found a constant (no shear dependent) slip length of 8-9nm for water on wetting mica and glass surfaces [72]. These dissimilar findings also did not agree with available theoretical results. However Ducker *et al.*, using an independant optical measurement of the probe-distance in the AFM,

found a regular no-slip BC on a similar system as the one investigated by Craig *et al.* [73]. It was recently shown by Craig *et al.* that the lateral tilt of the cantilever was a significant issue in interpreting hydrodynamic forces [74]. Vinogradova *et al.* also evidenced the important effect of the dissipation due to the cantilever [75]. Using a "snow-man" probe made of two spheres glued on the top of each other, they showed a perfect agreement with the no-slip BC on hydrophilic surfaces, confirming SFA experiments, and a moderate slip length of 10nm of water onto rough hydrophobic surfaces. Finally dynamic measurements using an oscillatory drive were implemented in the AFM by Maali *et al.* so as to measure the dissipation coefficient with high accuracy [76]. Using this technique they found a no-slip BC of water onto mica surface, and a 8nm slip length on atomically smooth HOPG graphite with contact angle 70° [77].

An alternative way to measure interfacial hydrodynamic dissipation is through the dissipation-fluctuation theorem, for instance by measuring the modification of the brownian motion of a probe at the vicinity of a surface. In Joly *et al.* experiment [22] the average transverse diffusion coefficient of colloidal particles confined in a liquid slab was measured by Fluorescence Correlation Spectroscopy as a function of the film thickness, and related to the boundary condition on the slab walls. A resolution better than 5nm is obtained with particles of 200nm nominal diameter, by averaging the data over 100000 events crossing the measurement volume. The originality of the method is to give access to the boundary condition without any flow, i.e. really at thermodynamic equilibrium. It is thus directly comparable to theoretical predictions. A collateral result is the direct probe of a property of great interest in nanofluidics, i.e. the motion of a solute close to a wall.

Besides the dissipative methods, great progress was achieved in the development of optical methods giving direct access to the flow field and its extrapolation to the solid wall with a sub-micrometer resolution.

The Micro-Particle Image Velocity (μ -PIV) technique has been widely used in microfluidics. First attempts to determine the BC yielded slip lengths of micrometer amplitude [78], difficult to conciliate with theoretical expectations, although the variation of slippage with the liquid-solid interaction were consistent. Gaining better resolution raised many issues. Besides colloidal forces acting on particles close to a wall, which have to be taken into account, such as DLVO forces or electro-osmosis induced by the streaming potential, an important source of uncertainty is the determination of the wall position: locating the latter from the signal of moving particles lead to a systematic bias because of the depletion induced by the colloidal lift [79]. By using the signal of non-moving particles adsorbed to the wall Joseph et al [80] increased the resolution on the slip length to 100nm in a configuration similar to [78], and found no slippage at this (100nm) scale whatever the wettability of the surface. A recent investigation using double-focus FCS confirmed the exis-

tence of slippage of a few ten nanometers on hydrophobic surfaces [81]. A major improvement toward nanometric resolution is the Total Internal Reflection Fluorescence method which uses an evanescent wave at the interface to be probed, and allow to measure the distance of a tracer particle to the wall through the exponential decay of the signal amplitude. Bouzigues *et al.* found a water slip length of 21nm (± 12 nm) on OTS coated glass capillaries [101], while Lasne *et al.* measured a water slip length of 45nm (± 15 nm) on a similar surface [82]. These results are consistent and the different values of slip length may well be ascribed to slight variations in surface preparation. Note that in such measurements, the size of the probe itself is a major issue in the race toward nanometric resolution: Brownian motion increases as the particle size decreases, not only adding noise to the measurement, but allowing particles to leave the focal plane between two successive images which decreases the locality of the measurement. Some specific statistical treatment has to be performed in order to avoid any bias in the estimated velocity [82, 83, 101].

A summary of the results obtained with water on various smooth surfaces is gathered in Fig.4 plotting the slip length as a function of the contact angle. The various methods show the same trend: water does not slip on hydrophilic surfaces, and develops significant slippage only on strongly hydrophobic surfaces. The highest slip lengths reach the range of 20-30nm: accordingly hydrodynamic slippage is non relevant in microfluidic devices, but of major importance in nanochannels. On this basis one expects that water flow in highly confined hydrophobic pores, such as mesoporous media or biological channels (*c.f.* the Aquaporin example in the introduction), should be much less dissipative than ordinary Poiseuille flow. The results obtained with the various methods show a very good qualitative agreement with theory and molecular dynamics simulations performed with water [45]. However the experimental slip lengths show a systematic bias toward higher values than theoretical ones. The discrepancy is actually not understood and might be the effect of gas adsorbed at the wall, possibly condensed in nanobubbles, an active research area recently [84, 85].

Finally, the case of organic molecules still raises debates. In the case of perfect wetting, various works on mica surfaces [13, 18], as well as on glass surfaces [14, 70], showed that alkanes and OMCTS have a no-slip velocity either at the wall or at a molecular size inside the liquid phase (negative slip length). However Pit *et al.*, using a fluorescence recovery method with molecular probes in a TIRF configuration, found very large slip lengths ($\simeq 100$ nm) of hexadecane and squalane on atomically smooth saphir surfaces although these liquids wet perfectly the saphir [87, 88]. Further work is under progress to understand if these large slip lengths in the case of favorable solid-liquid interactions reflect a particular effect of molecular structure and incommensurability at the saphir/liquid interface. More generally, although the

problem of the boundary condition has generated an important instrumental progress in the quantitative measurement and control of flows at a nanoscale, a full quantitative confrontation with the theory, *e.g.* Eq.(11), is still lacking.

IV. NANOMETRIC DIFFUSE LAYERS AND TRANSPORT THEREIN

The transport of electrolytes within the EDL and the associated phenomena have been extensively studied during the last century due in particular to its central role in colloid science. It has been accordingly discussed exhaustively in textbooks and reviews [42, 89] and in the present section we merely point to the main concepts which will be useful for our discussion.

In spite of this long history, new directions and perspectives have been opened very recently in this old domain. Novel insight into the nanometric Debye layer have indeed been reached: new tools now make it possible to investigate the detailed structure and dynamics *inside* the Debye layer. This concerns both the experimental side, see previous section, and numerical side, with the development of ever more powerful Molecular Dynamics tools.

From these more 'molecular' views of the EDL, in contrast to the more standard 'continuum' picture of the EDL, new concepts and phenomena have emerged. We shall thus merely focus here on the recent progress and new leads opened by nanofluidics in this domain.

A. From Debye layer to ion specific effects

An EDL builds up at a charged interface: it is the region of finite width where the surface charge is balanced by a diffuse cloud of counterions [89]. The Debye layer is usually described on the basis of the mean-field Poisson-Boltzmann (PB) theory, see [39] for a review. Ions are described as point charges and only their valency enters the description. Correlations between charges are accordingly neglected. The thermodynamic equilibrium balancing the ions entropy to their electrostatic interaction with the surface (attraction for the counter-ions and repulsion for the co-ions) leads to the introduction of the Debye length, as introduced above in Eq. (5) and which we recall here:

$$\lambda_D = (8\pi\ell_B\rho_s)^{-1/2} \quad (14)$$

Getting more into details, the PB description results from the combination of (i) the Poisson equation relating the electrostatic potential V to the charge density $\rho_e = e(\rho_+ - \rho_-)$ according to

$$\Delta V = -\frac{\rho_e}{\epsilon} \quad (15)$$

with ϵ the dielectric constant, here identified to its bulk value, and Δ the spatial Laplacian; and (ii) the thermodynamic equilibrium leading to a spatially constant electro-chemical potential for the ions:

$$\mu_{\pm} = \mu(\rho_{\pm}) \pm z_{\pm}eV \quad (16)$$

with z_{\pm} the ion valency, ρ_{\pm} the ion densities and under the above assumptions, $\mu(\rho) = \mu_0 + k_B T \log \rho$ the perfect gas expression for the chemical potential.

Though its crude underlying assumptions, the mean-field PB theory captures most of the physics associated with the EDL and is the usual basis to interpret ion transport. One reason for this success is that ion correlations within the EDL, which are discarded in PB, can generally be neglected. This can be quantified by introducing a coupling parameter, Γ_{cc} , which compares the typical inter-ions electrostatic interaction to thermal energy [90, 91]. Following Refs [90] and [91], the latter is estimated as $\Gamma_{cc} \approx e^2/(4\pi\epsilon\ell)/k_B T = \ell_B/\ell$, with ℓ the mean distance between ions at the surface. This scale is related to the charge density Σ , as $\ell \approx \Sigma^{-1/2}$, so that $\Gamma_{cc} \approx \sqrt{\Sigma\ell_B^2}$ [91]. PB is expected to break down when the coupling parameter exceeds unity. For typical surfaces this threshold is not reached: for glass, the surface charge is at most in the 10^{-2}C/m^2 range ($\sim 6.10^{-2} e/\text{nm}^2$), and the coupling parameter Γ_{cc} remains smaller than unity.

Other assumptions inherent to PB could be also questioned. In the PB description, the dielectric constant is assumed to be spatially uniform and identical to its bulk value. This assumption is expected to break down very close to surfaces, in particular hydrophobic, where water ordering induce a local electric dipole pointing outward to the interface [92]. This casts some doubts on the local relation between medium polarization and local electric field. However MD simulations suggest that using the bulk dielectric constant in Poisson equation is not a critical assumption and can be safely used to describe the EDL [92].

PB description however misses an important class of effects associated with the specific nature of ions, and which affect the fine structure of the EDL. Ion specificity is intimately connected to Hoffmeister effects, namely that the interactions between charged and neutral objects in aqueous media do depend crucially on the type of ion and not only on electrolyte concentration [93, 94, 95]. Such effects occurs not only at the air-water interface, where it does affect surface tension depending on ion type, but also at hydrophobic surfaces [94, 96]. This effect is evidenced in Fig. 5, where results of molecular dynamics simulations of ions dispersed in water (SPC-E model) from Ref. [96] demonstrate that iodide ions do strongly adsorb at air-water and hydrophobic interfaces, while chloride do not. Note that a EDL builds up even in the case of a neutral interface, we shall come back on this result and its implications. In general heavier halide ions adsorb at the hydrophobic surface. This effect is mostly absent at a hydrophilic interface. Tools of molec-

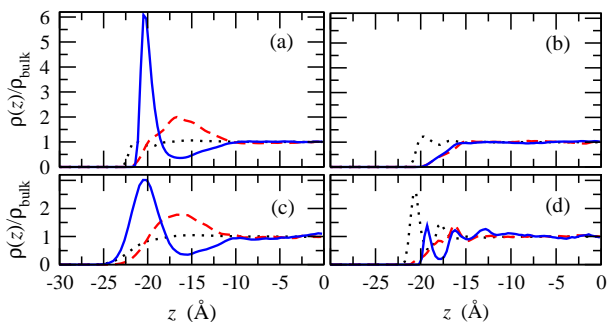


FIG. 5: Simulated density profiles of negative ions (solid lines), positive ions (dashed lines), and water (dotted lines) for roughly 1-M solutions of (a) NaI and (b) NaCl between neutral hydrophobic surfaces, (c) NaI at a vapor-liquid interface, and (d) NaI between neutral hydrophilic surfaces. From Ref. [96].

ular simulation and new spectroscopic techniques have fully renewed the interest in ion specific phenomena [95]. The origin of the effect involves many aspects, as ion polarizability, image-charge interaction, ion-size (steric) effects, dispersion forces and the mechanisms are still the object of intense research ... and also of some fierce debate, such as for the preferred adsorption of hydronium versus hydroxyl at interfaces[97], which fixes the charge of the liquid-vapor interface.

Such ion-specificity effects, which go beyond the traditional PB framework, have profound effects on the ion-transport process within the Debye Layer, which we explore in the next part.

B. Interfacial transport: Electro-osmosis , streaming currents, and beyond

The EDL is at the origin of various electrokinetic phenomena. Here we shall discuss more particularly electro-osmosis (and -phoresis for colloids) and its symmetric phenomena, streaming currents. Both phenomena take their origin in the ion dynamics within the EDL. Due to the nanometric width of the EDL, these phenomena are 'nanofluidic' by construction and the various lengths introduced in Sec.II will appear.

Let us first discuss electro-osmosis (EO). EO is the phenomenon by which liquid flow is induced by an electric field. In its simplest form, the fluid velocity v_f beyond the EDL is linearly connected to the applied electric field E_e according to the Smoluchowski formula [42]:

$$v_\infty = -\frac{\epsilon\zeta}{\eta}E_e \quad (17)$$

with ϵ the dielectric constant, η the viscosity and ζ the so-called zeta (electrostatic) potential. The common interpretation of ζ is that it is the electrostatic potential at the "shear plane", *i.e.* the position close to the wall

where the hydrodynamic velocity vanishes. As we now discuss, this interpretation should be taken with caution.

Let us briefly recall the derivation of Eq.17. Fluid dynamics is described by the stationary Stokes equation:

$$\eta \frac{\partial^2 v_x}{\partial z^2} + \rho_e E_e = 0 \quad (18)$$

Here we use a frame where the electric field E_e is along x and parallel to the planar surface, and the velocity field v_x only depends on the direction z perpendicular to it.

A key remark, already mentioned above, is that the charge density, $\rho_e = e(\rho_+ - \rho_-)$, is non vanishing only within the EDL, so that the driving force for fluid motion, $F_e = \rho_e E_e$ is limited to that nanometric region, and vanishes otherwise. In order to obtain the velocity profile, the Stokes equation should be integrated twice, and thus requires two boundary conditions. Far from the surface, the velocity profile is plug-like and $\partial_z v|_{z=\infty} = 0$. At the wall surface, the hydrodynamic boundary conditions for the hydrodynamic velocity profile should be specified. We have discussed above that the latter introduces a slip length b , according to Eq. 7, as $b \partial v|_{z=0} = v(z=0)$. Using Stokes and Poisson equations, one gets immediately that the full velocity profile is related to the electrostatic potential V as

$$v(z) = -\frac{\epsilon}{\eta} E \times [-V(z) + \zeta] \quad (19)$$

where ζ has the meaning of a zeta potential[153] and takes the expression

$$\zeta = V_0 \times (1 + b \cdot \kappa_{\text{eff}}) \quad (20)$$

where V_0 is the electrostatic potential at the wall and κ_{eff} is the surface screening parameter, defined as $\kappa_{\text{eff}} = -V'(0)/V_0$ [92, 98]. For weak potentials this reduces to the inverse Debye length: $\kappa_{\text{eff}} \simeq \lambda_D^{-1}$, but its full expression takes into account possible non-linear effects. The fluid velocity far from the surface (*i.e.* outside the EDL) has the Smoluchowski expression above, Eq. (17), with the expression of the zeta potential, ζ , given in Eq. 20. This prediction was first discussed in Ref. [99], and re-derived independently in more recent works [92, 98]. We emphasize that the above result, Eqs. (19-20), does not make any assumption on the specific model for the EDL, except for a constant dielectric constant ϵ and the validity of Stokes equation, which was discussed above to be valid down the nanometer.

The physical meaning of the above expressions is quite clear. The velocity in the fluid results from a balance between the driving electric force and the viscous friction force on the surface. Per unit surface, this balance writes

$$\eta \frac{v_\infty}{\lambda_D + b} \approx e\Sigma \times E \quad (21)$$

with Σ the surface charge density (in units of m^{-2}) at the wall. The expression for the viscous friction expresses the fact that flow gradients occur on a length $b + \lambda_D$.

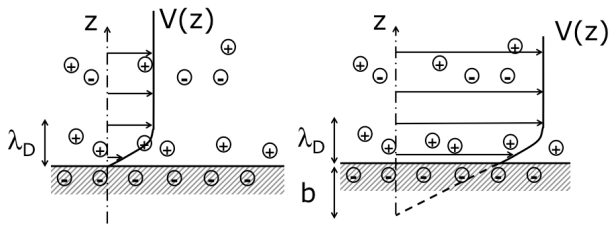


FIG. 6: Sketch of the influence of slippage on the electro-osmotic transport. Slippage reduces the viscous friction in the electric Debye layer, as the hydrodynamic velocity gradient occurs on a length $b + \lambda_D$, instead of λ without slippage. Flow is accordingly enhanced by a factor $1 + b/\lambda_D$.

Relating the surface charge to the surface potential V_0 ($e\Sigma = -\epsilon \partial_z V|_0$), one recovers the above results.

As a side remark, one may note that the slip enhancement does not require any assumption on the electric and fluid behavior. Indeed at a fully general level, the (exact) momentum balance at the surface shows that the velocity at the wall is *exactly* given by $v_{\text{wall}} = \frac{D_{\text{wall}}}{\lambda} E$, with D_{wall} the dielectric displacement computed at the surface, and λ the surface friction coefficient introduced in Eq.(9). The latter is related to slip length according to the definition $\lambda \equiv b/\eta$. This expression for the wall velocity under an applied electric field neither invokes Navier-Stokes equation, nor any assumption on the dielectric behavior. This wall velocity acts as a lower bound to the asymptotic EO velocity, *i.e.* the one measured at infinite distance from the surface. This demonstrates that the enhancement of the EO velocity due to low liquid-solid friction, *i.e.* large slippage, has a fully general validity.

Several conclusions emerge from the above equation. First if the wall is characterized by a no-slip BC, with $b = 0$, then the zeta potential ζ , Eq. (20) identifies with the electrostatic potential V_0 computed at the surface (up to a possible molecular shift due to the precise position of the hydrodynamic BC which defines the so-called shear plane [98]): this is the common assumption, as usually expressed in textbooks [42]. Now, if finite slippage occurs at the surface, then *the zeta potential is much larger than the surface electrostatic potential*, V_0 : it is amplified by a factor $1 + b/\lambda_D$ (assuming for the discussion that $\kappa_{\text{eff}} = \lambda_D^{-1}$). This factor may be *very large*, since on bare hydrophobic surfaces b may reach a few ten nanometers (say $b \sim 20 - 30\text{nm}$), while the Debye length typically ranges between 30 nm down to 0.3 nm (for 10^{-4}M to 1M).

These predictions have been confirmed by molecular Dynamics simulations of electro-osmosis (and streaming current, see below) [92, 96, 98]. Various systems were considered, from a model electrolyte involving ions in a Lennard-Jones solvent, to a more sophisticated SPC-E model of water, with ions of various nature. Altogether simulations confirm the key role of slippage on electrokinetics and results do fully confirm the above description.

On the experimental side, this strong influence of surface dynamics on the electrokinetics at surfaces has not been appreciated and explored in the electrokinetic literature up to now, and very few experimental investigations have been performed on this question [100, 101]. One key difficulty is that the above result for the zeta potential, Eq. (20), involves a strong entanglement between electrostatics, through surface potential, and fluid dynamics, through hydrodynamic slippage. In order to disentangle the two effects, two independent measurements of these quantities should in principle be performed. To our knowledge the first work on the subject was performed by Churaev *et al.* in Ref. [100], and results indeed suggested a slip effect, at the expense however of a rather uncontrolled assumption on the surface potential. More recently this problem was tackled in Ref. [101] using the nanoPIV tool discussed above. This setup allows for two independent measurements of ζ and V_0 , leading to an unambiguous confirmation of the above predictions of slippage effect on the zeta potential. Indeed both the velocity profile, which is fitted to Eq. 19, and the nanocolloid concentration profile, from which the surface potential is deduced on the basis of the electrostatic repulsion, are measured independently. Velocity profiles from Ref.[101] are displayed in Fig. 7. While the two surfaces under consideration (a hydrophilic glass and a silanized hydrophobic surface) had basically the same surface potential, a factor of two is found on the zeta potential under the conditions of the experiment. Results are consistent with a slip length of $\approx 40\text{nm}$. The factor of two for ζ/V_0 occurs here due to a Debye length of $\approx 50\text{nm}$ in the experimental condition of Ref. [101] (a large Debye length is required to investigate flow inside the Debye layer at the present spatial resolution, $\sim 20\text{nm}$, of the nanoPIV technique). As a side remark, note the large slip velocity at the wall in the slippy case in Fig.7: this is expected since according to Eq.19, the velocity at the surface is directly proportional to the slip length b , as $v(0) = -\frac{\epsilon}{\eta} E \times V_0 \frac{b}{\lambda_D}$ (assuming, to simplify, that $\kappa_{\text{eff}} \approx \lambda_D^{-1}$).

This result opens new perspective to make use of surface physico-chemistry in order to optimize electric-induced transport and control flow by surface properties. It was also argued that such slip-induced optimization would strongly enhance the efficiency of energy conversion devices based on electrokinetic effects [102, 103].

Besides slip effect, ion-specificity has also an important influence on the electro-osmotic transport. As we reported above, the structure of the EDL is affected by the nature of the ions under consideration, especially at hydrophobic walls (and air-water interfaces). This can be best seen by rewriting the expression for the zeta potential, in Eq.20, in a slightly different form:

$$\zeta = \frac{1}{\epsilon} \int_0^{\infty} (z' + b) \rho_e(z') dz' \quad (22)$$

with ρ_e the charge density. This expression *e.g.* comes from the double integration of the Stokes law. As seen in

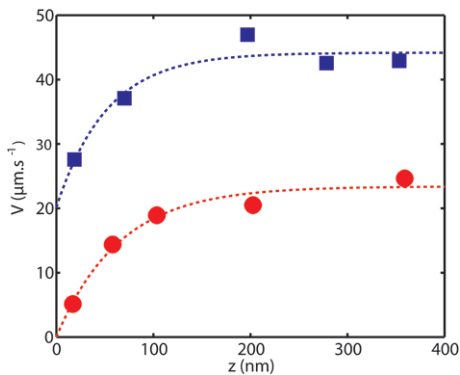


FIG. 7: NanoPIV measurements for the electroosmotic flows close to hydrophilic pyrex \bullet and hydrophobic OTS-coated surface \blacksquare . The deduced zeta potentials are $\zeta = -66 \pm 8\text{mV}$ (hydrophilic glass) and $\zeta = -123 \pm 15\text{mV}$ (hydrophobic, silanized surface), while the electrostatic potentials were independently measured to be comparable: $V_0 \simeq -69\text{mV}$ for the hydrophilic (pyrex) surface, and $V_0 \simeq -65\text{mV}$ for the hydrophobic (OTS-coated) surface. The salt concentration is $1.5 \cdot 10^{-4}\text{mol.L}^{-1}$ and the driving electric field is $E = 500\text{V.m}^{-1}$. Dashed lines are fits to the theoretical predictions using Eq. (19), with $\lambda_D = 51 \pm 10\text{nm}$ (measured independently) and $b = 0 \pm 10\text{nm}$ (bottom) and $b = 38 \pm 6\text{nm}$ (top) for the slip lengths. Figure from Ref. [101].

Fig. 5 ion specific effects have a strong influence on the charge distribution, and do indeed strongly modify the value of ζ . This effect was studied in various MD simulations of electrokinetics [92, 96, 104] and several counter-intuitive effects were indeed observed, such as flow reversal (as compared to the expected surface charge) [104], or even the existence of a non-vanishing zeta potential for a *neutral* surface [92, 96]! These effects can be understood from Eq. 22: while for a vanishing surface charge, the system is electro-neutral and $\int_0^\infty \rho_e(z') dz' = 0$, this however does not imply that its first spatial moment, which enters the expression of ζ according to Eq. 22, be zero.

More quantitatively, effects of ion-specificity on the zeta potential were rationalized in Ref. [92] on a basis of a minimal model, which was subsequently validated on MD simulations. This description is based on the idea that 'big' ions have a larger solvation energy and are therefore attracted to hydrophobic interfaces in order to minimize this cost [105]. An estimate of the solvation free-energy of ions close to interface allows to propose analytical predictions for ion-specific effects on the zeta potential.

We finally quote that all the above discussion on the electro-osmotic transport also applies to the streaming current phenomenon, by which an electric current is induced by the application of a pressure gradient. Again, since the EDL is not electro-neutral, liquid flow will induce an electric current inside the EDL [42]. According

to the Onsager symmetry principle, these two phenomena – electro-osmosis and streaming current – are intimately related and the cross coefficients should be identical. The expression for the streaming current I_e under an applied pressure gradient ∇P takes the form:

$$I_e = -\frac{\epsilon \zeta}{\eta} \mathcal{A}(-\nabla P) \quad (23)$$

where ζ takes the same expression as in Eq.(20) and \mathcal{A} is the cross area of the channel.

We end up this section by mentioning that the above effects generalize to any interfacial transport phenomena. Indeed the above electrically induced phenomena belong to a more general class of surface induced transport, which also involves phenomena known as diffusio-osmosis or thermo-osmosis and their associated phoretic phenomena for colloidal transport [21, 89]. Thermo-osmosis points to fluid motion induced by thermal gradients, while diffusio-osmosis corresponds to fluid flow induced by gradients in a solute concentration. Though relatively old, thermophoretic transport has been the object of recent investigations in particular for colloid manipulation [106, 107, 108]. Its origin is still the object of an intense debate with recent progress in disentangling the various contributions [106, 107, 109]. On the other hand, diffusio-phoretic and osmotic transport have been less explored [89, 110] but their potential in the context of microfluidic applications has been demonstrated recently [111, 112]. This opens novel possibility of driving and pumping fluids [112] – as well as manipulating colloids – with solute contrasts, which have been barely explored up to now and would deserve further investigations in the context of nanofluidics. A common point to all these phenomena is their “nanofluidic root”: as for the electro-osmotic transport discussed above, the driving force for fluid motion is localized within a diffuse layer of nanometric size close to the surfaces. Therefore, this opens the possibility of strongly amplifying their effect on the basis of slippage effects at the solid interface. As demonstrated theoretically in Ref. [113], the amplification is – as for electro-osmosis above – amplified by a factor $1 + b/\lambda$, where λ is the width of the diffuse layer. Similar effects are predicted for thermophoretic transport [114].

Finally, one may raise the question of interfacial transport on *super-hydrophobic* surfaces. Such surfaces, achieved using nano- or micro- engineering of the surfaces, were shown to considerably enhance the slippage effect and exhibit very large slip length in the micron (or even larger) range [46, 47, 115]. Accordingly, a naive application of the previous ideas would suggest massive amplification by a factor up to 10^4 (!). However, the composite structure of the superhydrophobic interface, involving both solid-gas and liquid-gas interfaces, makes these transport mechanisms far more complex in this case than on smooth interface. It has been shown that in the regime of thin Debye layer, no amplification is obtained for electro-osmosis on superhydrophobic surfaces

[112, 145], unless a non-vanishing charge exists at the liquid-gas interface. In contrast, a massive amplification is predicted for diffusio-osmosis [112]. This strong prediction has not received an experimental confirmation up to now.

Furthermore, a massive amplification, by a factor up to 10^4 (!), may be achieved when using nano-engineered surfaces associated with super-hydrophobic properties, which considerably enhance the slippage effect (with b raising to the micrometers range) [46, 47, 115].

C. Surface versus bulk: conductance effects

We now discuss the surface conductance effect in nanochannels.

The conductance, K , characterizes by definition the electric current versus electric potential drop relationship. As pointed out previously, conductance probes the number of free charge carriers, here ions. In the bulk K is therefore expected to be proportional to the salt concentration ρ_s (ionic strength). Now in the presence of surfaces, the charges brought by the surface lead to a supplementary contribution to the conductance.

Surface conductance is actually a rather classical phenomenon in colloid science [42], but it was demonstrated quite recently in the context of nanochannel transport by Stein *et al.* [41] and then by other groups [44].

As we introduced in Sec. II B 2.c, the ratio of bulk to surface charge carriers is characterized by the Dukhin length ℓ_{Du} . This length accordingly describes the competition between bulk and surface conductance. Depending on salt concentration, this length can be much larger than the Debye length. Surface conductance is therefore expected to dominate over the bulk contribution for nanochannels smaller than ℓ_{Du} . The magnitude of the surface conductance effect is amplified in small channels, but a key point is that it does not require Debye layer overlap.

Experimentally, the surface contribution to the conductance shows up as a saturation of the conductance in the limit of small salt concentration, while its expected bulk counterpart is expected to vanish in this limit. The saturation originates in the charge carriers brought by the surface charge, the number of which is independent of the salt concentration. This is illustrated in Fig. 8, from [41], where the conductance is measured in channels of various width, from 1015nm down to 70nm:

Let us discuss more specifically this point. In a slit geometry with width h , the general expression for the current (for a unit depth of the slit) takes the form

$$I_e = e \int_{-h/2}^{h/2} dz [\rho_+(z)u_+(z) - \rho_-(z)u_-(z)] \quad (24)$$

where the averaged velocities of the ions is

$$u_{\pm}(z) = v(z) \pm e\mu_{\pm}E_e, \quad (25)$$

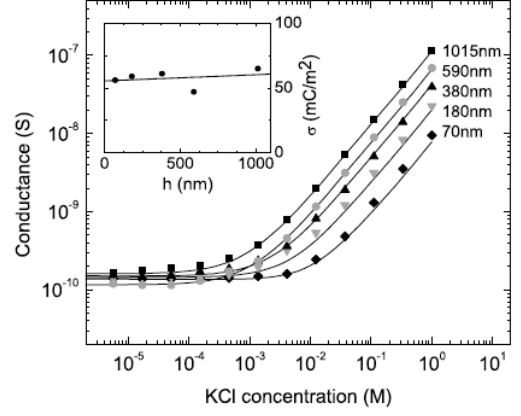


FIG. 8: Channel height dependence of ionic conductance behavior. The conductance of fluidic channels is plotted against salt concentration for various nanochannel width h ($h = 1015, 590, 380, 180,$ and 70 nm). The inset displays the fit values for the surface charge at the nanochannel walls as a function of h , from Ref. [41].

with μ_{\pm} is the ion mobility, defined here as the inverse of the ion friction coefficient (we assume furthermore $\mu_{\pm} = \mu$). The velocity $v(z)$ is the fluid velocity induced by electro-osmosis under the electric field, as given in Eq.(19). The second term is the contribution to the current due to ion electrophoresis.

Combining the expression of the velocity $v(z)$, as in Eq.(19), to Eqs. (24-25), one may remark that the electro-osmotic contribution to the current takes the form of the integral of the charge density times the electrostatic potential: this has therefore the form of an electrostatic energy, \mathcal{E} . This is confirmed by the full calculation, which leads to a conductance expression in the form [41, 116]:

$$I/E_e = 2e^2 \mu \rho_s \mathcal{A}(1 + H) \quad (26)$$

with \mathcal{A} the channel cross section ($\mathcal{A} = w \times h$ with w the depth of the channel) and the surface correction H

$$H = \cosh\left(\frac{eV_c}{k_B T}\right) - 1 + \frac{\mathcal{E}}{2\rho_s k_B T h} \left(1 + \frac{1}{2\pi\ell_B \mu \eta}\right) \quad (27)$$

where $V_c = V(0)$ is the electrostatic potential at the center of the channel, and $\mathcal{E} = \frac{\epsilon}{2} \int_{\text{slit}} dz \left(\frac{dV}{dz}\right)^2$ the electrostatic energy (and not the *free* energy). Note that writing $\mu = 3\pi\eta d_i$ with d_i the ion diameter, the last term in Eq.(27) is typically of order d_i/ℓ_B . It originates in the surface-induced – electro-osmotic – contribution to the conductance.

In the low salt concentration regime, $\rho_s \rightarrow 0$, the length scales are organized in the order:

$$\ell_{GC} < \lambda_D < \ell_{Du}, \quad (28)$$

since $\lambda_D/\ell_{GC} = \ell_{Du}/\lambda_D \gg 1$ for $\rho_s \rightarrow 0$. Saturation will occur as the channel width h is smaller than the Dukhin

length, $h < \ell_{Du}$, independently of the order of the h and λ_D . Debye layer overlap is accordingly *not* the source of the saturation of the conductance. In this regime, the second term in Eq. (27), associated with surface contributions is dominant.

In this limit, the calculation of the electrostatic energy shows that $\mathcal{E} \sim |\Sigma|$. The fact that \mathcal{E} scales linearly in $|\Sigma|$ and not as $|\Sigma|^2$ – as would be first guessed – is due to the non-linear contributions to \mathcal{E} in the Poisson-Boltzmann description. These become dominant in the $\rho_s \rightarrow 0$ limit where the Debye length becomes larger than the Gouy-Chapman length. Altogether, this shows that for $\rho_s \rightarrow 0$, the conductance saturates at a value

$$K_{\text{sat}} \approx e^2 \mu w \times 2|\Sigma| \left(1 + \frac{1}{2\pi\ell_B \mu \eta} \right) \quad (29)$$

with w the depth of the channel. This value is independent of both h and ρ_s . This saturation can be also partly understood in the context of Donnan equilibrium discussed below. In the limit $\rho_s \rightarrow 0$, only the counterion contributes to the ion concentration in the channel, $\rho_+ + \rho_- \approx 2\Sigma/h$, see Eq.(34) below, so that the conductance reduces to $K_{\text{sat}} \approx e^2 \mu w 2|\Sigma|$. This analysis however misses the electro-osmotic contribution to the conductance (second term in the brackets in Eq. (29)).

A few remarks are in order. First, the dependence of the conductance on the surface properties, here the surface charge Σ , opens new strategies to tune the nanochannel transport properties, *via* an external control. This has been used by Karnik *et al.* to develop a nanofluidic transistor [5], allowing to control the conductance of the nanochannel thanks to a gate voltage.

Another interesting remark is that along the same line as in Sec. IV B, the electro-osmotic contribution to the conductance could be also amplified by slippage effects. This can be readily demonstrated by a direct integration of Eq. (24). Accordingly slippage effects add a new contribution to the conductance:

$$K_{\text{slip}} = 2e^2 w \frac{\Sigma^2}{\eta} \times b \quad (30)$$

Assuming Stokes law for ion inverse mobility ($\mu = (3\pi\eta d_{\text{ion}})^{-1}$ with d_{ion} the ion size), then $K_{\text{slip}}/K_{\text{sat}} \sim b \times d_{\text{ion}} |\Sigma| \approx b/\ell_{GC}$: since the Gouy-Chapman length ℓ_{GC} is typically nanometric (or less), this enhancement is therefore very large, even for moderate slip length ($b \sim 30\text{nm}$) !

The channel resistance is accordingly decreased by the same factor in the low salt regime. This amplification of conductance by hydrodynamic slippage opens very interesting perspectives in the context of electrokinetic energy conversion, as was pointed out recently by Pennathur *et al.* [103] and Ren and Stein [102]. Moderate slippage, with slip length of a few ten nanometers, is predicted to increase the efficiency of the energy conversion up to 40% (and of course even more with larger slip lengths). This attracting result would deserve a thorough experimental confirmation.

D. Debye layer overlap and nanofluidic transport

The phenomenon of Debye layer overlap has already been widely explored in the nanofluidic literature. As we pointed above, various reasons underlie this specific interest: (i) well controlled nanometric pores with size in the range of 20-100 nm can be produced using micro-lithography techniques [40]: this does indeed correspond precisely to the range of typical Debye lengths for usual salt concentrations (remember that $\lambda_D = 30\text{nm}$ for a salt concentration of 10^{-4}M); (ii) the overlap of Debye length does indeed have a strong influence on ion transport, so that novel transport effects emerge at this scale, with applications for chemical analysis.

The question of Debye layer overlap, and related phenomena, was discussed quite extensively in a recent review by Schoch *et al.* [40]. Here we thus focus on the main guiding lines underlying this problem and point to the key physical phenomena at play. In particular we shall discuss an illuminating analogy to transport in semiconductors.

1. Donnan equilibrium

An important notion underlying the Debye overlap is the so-called ‘‘Donnan equilibrium’’, which is a well know concept in the colloid literature. Due to the supplementary charges brought by the nanochannel’s surface, a potential drop builds up between the nanochannel’s interior and the external reservoir, in order to maintain a spatially uniform chemical potential of the ions. The latter, as introduced above, takes the form (assuming a dilute ion system):

$$\mu(\rho_{\pm}) = \mu_0 + k_B T \log(\rho_{\pm}) \pm eV = \mu_0 + k_B T \log(\rho_s) \quad (31)$$

with ρ_s the (uniform) salt concentration outside the nanochannel, *i.e.* the ‘‘reservoir’’. These equations are completed with the overall electroneutrality over the channel,

$$\int_{-h/2}^{h/2} dz (\rho_+(z) - \rho_-(z)) = 2\Sigma \quad (32)$$

with z along the direction perpendicular to the nanochannel (here assumed to be a slit), see Fig. 9.

We now focus on the thin pore limit, assuming Debye layer overlap $h \lesssim 2\lambda_D$. In this situation, ion densities and electrostatic potential are approximately spatially uniform over the pore thickness h . Ion densities thus obey:

$$\begin{aligned} \rho_+ \times \rho_- &= \rho_s^2 \\ \rho_+ - \rho_- &= \frac{2\Sigma}{h} \end{aligned} \quad (33)$$

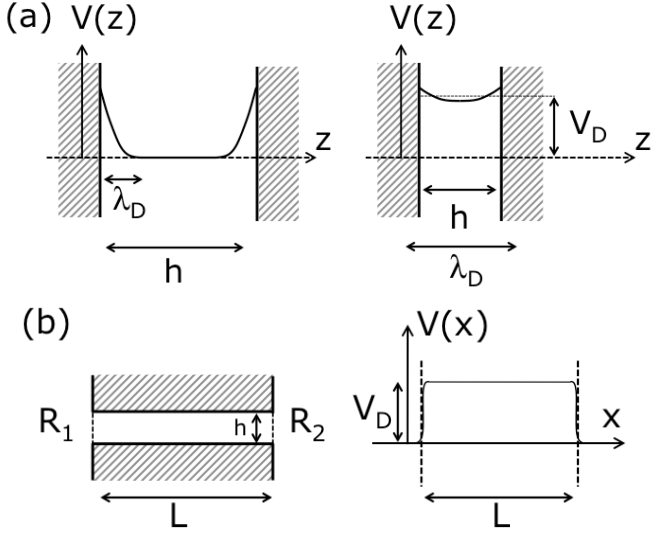


FIG. 9: (a): Sketch of the electrostatic potential in a charged slit with thickness h : (left) $h > 2\lambda_D$; and (right), $h < 2\lambda_D$, corresponding to Debye layer overlap. (b) A charged nanochannel, with thickness h and length L , connects two reservoirs R_1 and R_2 . In the situation of Debye layer overlap, a Donnan potential V_D builds up along the nanochannel.

Altogether, this leads to

$$\begin{aligned} \rho_{\pm} &= \sqrt{\rho_s^2 + \left(\frac{\Sigma}{h}\right)^2} \pm \frac{\Sigma}{h} \\ V_D &= \frac{k_B T}{2e} \log \left[\frac{\rho_-}{\rho_+} \right] \end{aligned} \quad (34)$$

where the mean electrostatic potential V_D is denoted as the Donnan potential.

Note that the amplitude of the Donnan potential V_D is quantified by the ratio ℓ_{Du}/h where $\ell_{Du} = \Sigma/\rho_s$ is the Dukhin length introduced above. To fix ideas $\ell_{Du} \sim 1nm$ for $\rho_s = 1M$ and a typical surface charge.

It is finally of interest to mention the strong analogy between the Donnan equilibrium and the equilibrium of charge carriers in doped semi-conductors (SC). In the latter the electrons density ρ_n and the holes density ρ_p obey Eq. (33) with the electrolyte density ρ_s replaced by the carriers density in the intrinsic (non-doped) SC. The surface charge in the nano-channel actually acts as impurities delivering additional carriers, with $\Sigma > 0$ corresponding to donors (N-doped SC) and $\Sigma < 0$ acceptors (P-doped SC). The Donnan potential is then the analogous of the shift in the Fermi energy due to impurities, which determines the voltage difference at equilibrium between regions of different dopage level. The table hereafter, table I, summarizes the corresponding quantities in the nano-channel and SC analogy.

The Donnan potential and Debye layer overlap have many implications on nanofluidic transport.

Nanofluidics	Semi-conductors
ρ_- negative ions concentration	ρ_n electron density in the conduction band
ρ_+ positive ions concentration	ρ_p holes density in the conduction band
ρ_s electrolyte concentration	n_i carriers density in the intrinsic SC
surface charge $2\Sigma/h$	Impurities (dopping) concentration
Donnan potential	Shift of the Fermi level

TABLE I: Equivalence table for corresponding quantities in doped semiconductors and nano-channels.

2. Ion transport and PNP equations

A classical framework to discuss ion transport in narrow pores is the so-called Poisson-Nernst-Planck (PNP) equations. This simplified description of ion transport in strongly confined channels is based on the coupled diffusion-electro-convection of the ions [117].

As in Fig.9, the channel thickness is assumed to be small compared to the Debye length, $h \ll \lambda_D$, so that ion concentrations are assumed to be uniform across its thickness. The ion fluxes J_{\pm} (per unit surface) then takes the form

$$J_{\pm} = -D_{\pm} \partial_x \rho_{\pm}(x) \pm \mu_{\pm} e \rho_{\pm}(x) (-\partial_x V)(x) \quad (35)$$

where D_{\pm} and μ_{\pm} are related by the Einstein relationship, $D_{\pm} = \mu_{\pm} k_B T$; x is along the direction of the channel. Note that for simplicity, a single salt and monovalent ions are considered here. A local version of the electroneutrality, Eq. (33), may be made along the pore:

$$\rho_+(x) - \rho_-(x) = \frac{2\Sigma(x)}{h} \quad (36)$$

Finally at the pore entrance and exit, a Donnan electric potential drop builds up, along the description given above, see Eq. (34).

To illustrate further this approach, we consider the transport through a single nanochannel, as sketched in Fig.9-b. At equilibrium the two reservoirs, R_1 and R_2 have the same electric potential and salt concentration, associated with a uniform Donnan potential along the channel. Now if an electrostatic potential drop ΔV or a salt concentration difference $\Delta \rho_s$ is imposed between the reservoirs, ion fluxes will build-up so as to relax towards equilibrium.

In the stationary state, the ion flux are spatially uniform, so that one may solve Eqs. (35-36) for the ion densities and electrostatic potential. This allows to compute the current $I = \mathcal{A}e(J_+ - J_-)$ and total ion flux $\Phi_t = \mathcal{A}(J_+ + J_-)$, with \mathcal{A} the cross area. In general, the relationship $I(\Delta V, \Delta \rho_s)$, $\Phi_t(\Delta V, \Delta \rho_s)$ are non-linear.

However, in the limit of small ΔV and $\Delta \rho_s$, a linear relationship can be written in general between the ionic fluxes and corresponding thermodynamic 'forces' [119, 120]:

$$\begin{bmatrix} I \\ \Phi_t \end{bmatrix} = \frac{\mathcal{A}}{L} \begin{bmatrix} K & \mu_K \\ \mu_K & \mu_{\text{eff}} \end{bmatrix} \begin{bmatrix} -\Delta V \\ -k_B T \Delta[\log \rho_s] \end{bmatrix} \quad (37)$$

with \mathcal{A} the cross area of the channel and $\Delta[\log \rho_s] = \Delta\rho_s/\rho_s$. Note that due to Onsager (time reversal) symmetry, the non diagonal coefficients of the matrix are equal [119, 120].

The coefficients of the above matrix can be calculated within the PNP framework. PNP equations are solved analytically for small potential and concentration drops, leading to the following expression for the various coefficients in the matrix, Eq.(37):

$$\begin{aligned} K &= 2\mu e^2 \sqrt{\rho_s^2 + \left(\frac{\Sigma}{h}\right)^2} \\ \mu_{\text{eff}} &= 2\mu \times \sqrt{\rho_s^2 + \left(\frac{\Sigma}{h}\right)^2} \\ \mu_K &= e\mu \times \frac{2\Sigma}{h} \end{aligned} \quad (38)$$

We assumed here that ions have the same mobilities $\mu_{\pm} = \mu$. The cross effects, associated with the mobility μ_K , originate in the dependence of the Donnan potential on the salt concentration.

Let us conclude this part with a few remarks:

- First one should realize that a number of assumptions are implicitly made in writing PNP equations. In particular the ions are treated as a perfect gas and correlations between ions along the channel are neglected. This may become problematic in strongly confined situations where single file transport (of the solvent) and strong unidirectional electrostatic correlations should build up. As an example, proton transport in single file water has been shown to involve a highly-cooperative mechanism [118]. However these limitations are restricted to single file transport in molecular channels, and should not be a limitation for pore size larger than a nanometer. Furthermore the PNP model is interesting to explore as guiding line, in the sense that it provides a rather correct physical idea of the (complex) electro-diffusion couplings.

- Furthermore, we may pursue the analogy discussed above between nanochannels and doped SC (see Table I), and extend the discussion to transport phenomena. Indeed **the Poisson-Nernst-Planck equations, Eqs.(35), are formally identical to the phenomenological transport equations for electrons and holes in SC**. Thus, as long as electrical and concentration fluxes *only* are allowed, *nanofluidic devices can in principle reproduce standard SC-based components*, such as diodes and transistors. The nanofluidic diode for instance is based on the properties of a PN junction, *i.e.* the junction between two regions with different doping: according to the equivalence table, Table I, its nanofluidic equivalent corresponds to two nanochannels with different surface charge Σ/h . We will discuss below (paragraph

5) some recent findings confirming the pertinence of this analogy.

- However one should keep in mind that the transport analogy between fluids and electrons breaks down in the presence of an hydrodynamic flow. Actually, PNP equations introduced above do not take into account convective contributions. In a fluidic system, a flow is indeed expected to occur in nanochannels as soon as a voltage drop is applied to its end, due to the body force acting on the mobile charges, but also under a pressure gradient (hydrostatic or osmotic). This is for example the source of electro-osmotic or streaming current contributions discussed above. In contrast, SCs can not flow - quite obviously - under an applied electric field and may only deform elastically. This is therefore a limitation to the above analogy.

Beyond this analogy to SC transport, the above PNP equations do not involve any hydrodynamic contributions. This concerns for example the electro-osmotic contributions (see *e.g.* the very last - viscosity dependent - term in the expression of the conductance, Eq.(27)), or the slip-induced enhancement of these phenomena. These may well become dominant in the strongly confined regime for sufficiently large slippage. In general a convection contribution to the ion flux should therefore be added to the above ion flux, in the form $J_{\text{conv}}^{\pm} = v_f \times \rho_{\pm}$, where v_f is the water velocity. The water velocity is in turn coupled to (electric) body forces via the momentum conservation equations, in practice the Navier-Stokes equation in its domain of validity. Altogether, the hydrodynamically induced cross phenomena, *i.e.* electro-osmosis, streaming currents, diffusio-osmosis, ... (as well as bare osmosis), can be summarized at the linear level in terms of a symmetric transport matrix, in a form similar to Eq. (37). This matrix relates linearly the fluxes to thermodynamic forces at work [120, 121, 122]. These phenomena have been discussed extensively in the context of membrane transport but generalize here to transport in nanofluidic channels.

More generally the coupling of the ion transport to the fluid transport thus opens the route to new applications in nanofluidic devices, with a richer phenomenology than in SC electronics.

We now illustrate the above concepts on a few practical situations.

3. Permselectivity

As a first example, we consider the permeability of nanopore to ions. It was first shown by Plecis *et al.* [2] that nanochannels exhibit a selective permeability for ion diffusive transport, see Fig. 10(a): ions of the same charge as the nanochannel surface (co-ions) exhibit a lower permeability, while ions of the opposite charge

(counter-ions) have a higher permeability through the nanochannel.

This charge specific transport is a direct consequence of a non-vanishing Donnan potential in the nanochannel (and Debye layer overlap). As pointed out above, Fig. 9, counter ions exhibit a higher concentration in the nanochannel as compared to that of a neutral specie, $\rho_+ > \rho_n$, while co-ions have correspondingly a lower concentration, $\rho_- < \rho_n$.

The diffusive flux of counter-ion will be accordingly larger than its expectation for neutral species, and vice-versa for co-ions. This leads therefore to a charge-specific effective diffusion coefficient D_{eff} for the co- and counter-ions.

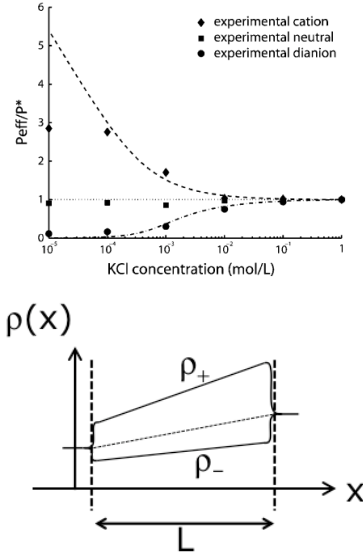


FIG. 10: *Top* Variation of the relative permeability of various probes with different charges, versus ionic strength. The experimental results are compared to theoretical fittings obtained with Eq. (40) (dotted lines). *Bottom* Concentration profiles of counter- and co-ions, ρ_{\pm} , for a given salt concentration drop $\Delta\rho$ between the two ends of the nanochannel. The dotted line represents the linear concentration profile for noninteracting diffusing species, whereas plain lines show the ion profiles in the nanochannel. Adapted from Ref. [2].

Following Plecis *et al.* [2], the effective diffusion coefficient is defined according to the identity

$$J_{\pm} = -D \frac{\Delta\rho_{\pm}}{L} \equiv -D_{\text{eff}} \frac{\Delta\rho}{L} \quad (39)$$

taking into account the fact that the local concentration in the nanochannel differs from the one imposed at the two ends of the reservoir. The linearized Poisson-Boltzmann equation is then used to calculate the ion concentration in the slit, ρ_{\pm} , as:

$$\beta_{\pm} = \frac{\bar{\rho}_{\pm}(x)}{\rho(x)} = \frac{1}{h} \int_{\text{slit}} dz \exp[\mp eV(z)/k_B T] \quad (40)$$

$$D_{\text{eff}}/D = \beta_{\pm}$$

with $\bar{\rho}_{\pm}(x)$ the (local) ion concentration in the nanochannel, averaged over the channel width h ; q the ion charge; $\rho(x)$ the local salt concentration in absence of electrostatic interactions (fixed by the salt concentration in the reservoirs); and $V(z)$ the electrostatic potential across the channel, for which Plecis *et al.* used a (linearized) Poisson-Boltzmann expression. A very good agreement with experimental results is found, as shown in Fig. 10, showing that this exclusion-enrichment picture does capture the essential ingredients of the ion diffusive transport. Note that using the Donnan description above, one may furthermore approximate the electrostatic potential by its Donnan expression in Eq.(34). This leads to an analytical expression for β_{\pm} as

$$\beta_{\pm} = \left(\frac{\rho_{\pm}}{\rho_{\mp}} \right)^{1/2} \quad (41)$$

where, as shown in Eq.(34), $\rho_{\pm} = \sqrt{\rho_s^2 + \left(\frac{\Sigma}{h}\right)^2} \pm \frac{\Sigma}{h}$. This expression reproduces the results in Fig. 40.

Finally, one should note however that due to the difference in ion permeability, a charge separation will build up between the two ends of the channel. This leads therefore to the creation of a reacting electric field along the channel, which will compensate dynamically for this charge separation [2]. This points to the complex couplings associated with charge transport in nanochannels. More experimental and theoretical work is certainly in order to get further insight in these phenomena.

4. Pre-concentration

Along the same lines, another consequence of Debye layer overlap is the 'pre-concentration' phenomenon, which was first observed by Pu *et al.* [3], and others [123]. Instead of a concentration drop as above, a voltage drop is applied along the nanochannel. It is then observed that ions enrich at one end and deplete at the other end. This phenomenon is illustrated in Fig. 11.

As above, a key point underlying the phenomenon is that ions of the opposite sign to the channel's surface, counter-ions, are more heavily transported than co-ions. This will create an enriched/depleted zone for both ions at the two ends of the channel.

This phenomenon has attracted a lot of interest, due in particular to its potential applications in the context of chemical analysis, for which it would provide a very interesting way of enhancing the sensitivity of detection methods.

At a basic level, the origin of preconcentration is a "cross effect" as introduced in Eq. (37): an electric potential drop ΔV leads to a flux of ions (Φ_t), as quantified by the cross-mobility μ_K . According to the PNP result for μ_K ($\mu_K = e\mu \times 2\Sigma/h$), this cross effect is thus a direct consequence of confinement and the existence of surface charges. Accordingly the magnitude of its effect, as com-

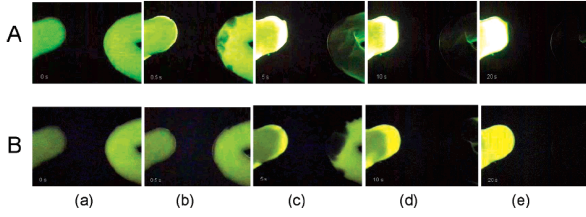


FIG. 11: Two micro-channels filled with fluorescent probes are connected by a nanochannel (a). After an electric field is applied across the nanochannels, an ion-enrichment and ion-depletion occurs at each end of the nanochannel (b-e). Figures (a) to (e) show the evolution of the fluorescence in the microchannel versus time (from 0 to 20 s). The probe used was (A) fluoresceine, (B) rhodamine 6G. From Ref. [3].

pared *e.g.* to the diffusive flux, depends on the Dukhin number, see Eq.(38).

But the detailed mechanisms underlying the preconcentration involve non-linear couplings between the various transport process of ions in the nanochannel, which are quite complex to rationalize. A systematic description of the phenomenon was proposed by Plecis *et al.* in Ref.[124], revealing the existence of various preconcentration regimes. We refer to Ref.[40] for a detailed discussion on the mechanisms underlying this process.

5. More complex functionalities: nanofluidic diodes

The analogy with transport in semiconductors quoted above suggest that more complex nanofluid transport phenomena can be obtained in the regime of Debye layer overlap.

We discuss here the analog of a PN junction in SC transport. Using the equivalence table, Table I, a PN junction corresponds for nanofluidic transport to a nanochannel exhibiting a disymetric surface charge along its surface.

Such a nanofluidic diode device has been developed by Karnik *et al.* [6], following a previous work by Siwy *et al.* in a different pore geometry [7]. This is illustrated in Fig.12 from Ref. [6]. The surface of a nanochannel is coated with two different surface treatments (half with avidin, half with biotin), leading to a surface charge contrast along the two moieties of the channel, Fig. 12-*Left*. Accordingly the current versus applied electric potential drop characteristics is found to exhibit an asymmetric shape: as in a classical diode, the current passes only in one direction. Similar asymmetric I-V curves are obtained for pores with asymmetric geometries, like conical pores obtained by track-etch techniques [7].

At a more quantitative level, Karnik *et al.* discussed the effect on the basis of the PNP equations discussed above, under the assumption of local electroneutrality. In the present disymetric case, Karnik *et al.* solve nu-

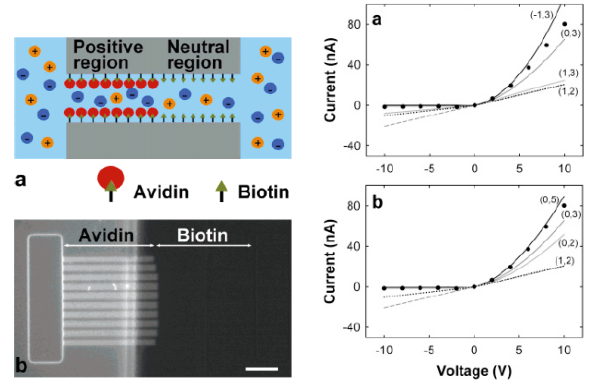


FIG. 12: *Left* (a) A nanofluidic diode is fabricated by patterning a nanochannel with different coating on its two moieties (avidin and biotin here). (b) Epifluorescence image of the fabricated nanofluidic diode, showing fluorescently labeled avidin in half the channel. Scale bar 20 μm . *Right* current versus applied voltage. Symbols are experimental data, while the solid lines are theoretical predictions using a PNP transport model. From Ref. [6].

merically these PNP equations for an applied potential drop at the ends of the pore [6]. Solutions are shown in Fig. 12, demonstrating that the PNP framework is indeed able to capture the transport rectification measured experimentally.

This diode behavior can also be discussed in the context of the analogy with semiconductor transport that we put forward above. The geometry described in Fig. 12 is indeed equivalent to that of a classical PN junction, corresponding to two regions with different doping. In the present case of a nanofluidic diode, the doping contrast between the P and N regions is associated with the different surface charge between the two moieties of the nanochannel. The diode effect in PN junctions is classically interpreted in terms of the Space-Charge Zone at the interface between the two regions with different doping. An approximate solution of the PNP equations can be proposed and leads to a rectified I-V characteristic which takes the form of the so-called Shockley equation [125]

$$I = I_S \left(\exp \left[\frac{eV}{k_B T} \right] - 1 \right) \quad (42)$$

where I_S is the so-called the saturation current I_S . This expression is expected to describe well the blocking to non-blocking transition of the junction, *i.e.* for moderate $eV/k_B T$. However this expression strongly overestimates the current at large $eV/k_B T$ for which a full solution of the PNP equations is needed.

In the Shockley equation, Eq.(42), the saturation current is expressed in terms of the donor-acceptor densities, ρ_A and ρ_D , as

$$I_S \approx eA n_i^2 \left(\frac{D_n}{L_n \rho_A} + \frac{D_p}{L_p \rho_D} \right) \quad (43)$$

where n_i is the carriers density, D_n , D_p the diffusion coefficients of electrons and holes, and L_n , L_p the length of the P and N regions. Using the equivalence table, Table I, one may convert this expression for the ionic transport using $D_n = D_-$, $D_p = D_+$, $L_n = L_p = L/2$, while $\rho_A = 2|\Sigma_A|/h$ and $\rho_D = 2|\Sigma_D|/h$.

This Shockley expression predicts an I-V curve in qualitative agreement with the experimental result in Fig. 12. However, quantitatively it does (very strongly) overestimate the current for large voltages V , as expected due to the simplifying assumptions underlying the expression in Eq. (42).

The analogy is however interesting to capture the underlying physics behind ion rectification in ionic transport. It allows to predict a full zoology of fluidic functionalities, in line with their SC analogues.

Finally it is interesting to quote that the disymetry measured here for I-V characteristics generalizes to other transport phenomena. For example, Siwy *et al.* also demonstrated the occurrence of a disymmetric diffusion of ions through conical pores [126].

Altogether these phenomena demonstrate the richness and complexity of behaviors obtained in the regime of Debye layer overlap. This definitely shows the great potential of nanofluidics, where further phenomena should emerge in the future taking benefit of these couplings.

V. THERMAL FLUCTUATIONS

In this section we raise the question of the role of thermal fluctuations in nanofluidic transport. As a general statistical rule, when the size of the system decreases, fluctuations play an increasingly important role. But under which conditions do they play a role? and which role could they play in nanofluidic transport?

There are quite a few studies on this question in relation to nanofluidic transport. One may cite the experimental study of noise in solid state nanopores by Dekker *et al.* [127]. The question of thermal fluctuations was also discussed in the context of numerical molecular dynamics simulations of osmotic flow through carbon nanotubes by Hummer *et al.* [128, 129]. Simulations show that – in the single file regime – the flow rate is essentially governed by thermal fluctuations rather than hydrodynamics. Hummer *et al.* proposed a 1D random walk to describe the nanofluidic water flow in this stochastic regime. Now, it is fair to remark that fluctuations are indeed expected to play a key role for single file transport, for which dynamics are highly correlated.

Aside from this situation, various indications of the role of thermal fluctuations have been reported, especially in studies involving capillary dynamics. One may cite the noise effects in the breakup of fluid nanojets by Mosler and Landman [130], the noise assisted spread-

ing of drops [131], and the influence of thermal noise in thin film dewetting [132] in relation to experiments [133]. In these different cases, thermal noise modifies quite strongly the dynamics, even at relatively large length scales (up to typically 100nm in Ref.[132]). These different situations can be described within the framework of fluctuating hydrodynamics [134], in which a random stress tensor is added to the Navier-Stokes terms. While this approach is indeed fruitful in describing the role of thermal fluctuations, a general criterion to quantify the importance of noise is however lacking.

Here, to illustrate the potential importance of fluctuations, we consider a simple situation in which an osmotic flow is driven across a single nanopore. The pore has diameter d and length L and is *impermeable* to the solute. The pressure drop across the membrane is $\Delta p = k_B T \Delta c$, with c the solute concentration. Under the pressure drop Δp , a fluid flow is induced, with mean velocity \bar{u} . Assuming NS equations to hold gives $\bar{u} \sim \frac{d^2}{\eta} \frac{\Delta p}{L}$. The flow is in the direction of higher solute concentrations.

Now one may ask the question: could fluctuations yield a reverse flow, *i.e.* against the pressure drop, at least for a short time? This would be clearly a (punctual) violation of second law. And what is the minimal size at which this may occur? A lead to such questions is provided by the so-called Fluctuation Theorem, which quantifies the probability of second law violation by fluctuations. This domain is presently a very active, in particular in the context of single molecule spectroscopy [135]. The theorem states that the probability $P(Q_\tau)$ to find a value Q_τ of the amount of heat dissipated in a time interval τ satisfies in a non-equilibrium state [136, 137, 138]

$$P(Q_\tau)/P(-Q_\tau) = \exp(Q_\tau/k_B T) \quad (44)$$

In the nanofluidic situation, this theorem would thus quantify the probability of a flow *against* the osmotic gradient. Let us compute the order of magnitude for the averaged \bar{Q}_τ in the stationary state: $\bar{Q}_\tau \approx \bar{F} \times \bar{u} \times \tau$, with F the frictional force acting on the nanopore surface. One has $F = \pi d L \sigma_w$ with σ_w the stress at the wall given by $\sigma_w \sim d \Delta p / L$. To fix ideas, we compute the amount of heat dissipated over a time needed for a molecule to pass through the whole pore, *i.e.* $\tau = L/\bar{u}$. Altogether this gives

$$\bar{Q}_\tau \sim \Delta p \times \mathcal{V} \quad (45)$$

with $\mathcal{V} = \frac{\pi}{4} d^2 L$ the volume of the pore. According to Eq. (44), violations of the second principle are more likely to occur when \bar{Q}_τ is of the order of the thermal energy. Putting numbers, if we choose $\Delta c = 1M$ (close to physiological conditions), then the condition $Q_\tau \sim k_B T$ is obtained for *nanometric* volumes, *i.e.* for a pore with a size (diameter, length) typically in the nanometer range. This is indeed typically the order of magnitude for the size of biological pores.

The occurrence of such 'counter flow' fluctuations has actually been observed in MD simulations of osmotic

flows through carbon nanotube membranes by Hummer *et al.* [128], and a stochastic model was proposed to account for the water transport across the tube. The above analysis thus fixes the limit where fluctuations starts to be predominant over the mean behavior.

Finally we note that one may perform the same estimate for a different situation of an electric current induced by an electrostatic potential drop ΔV . Assuming a bulk conductance, the dissipated heat is estimated under quite similar terms as $\bar{Q}_\tau \sim e\Delta V \times \rho_s \mathcal{V}$, with ρ_s the salt concentration. Again the condition $Q_\tau \sim k_B T$ is achieved for *nanometric* volumes.

These results point to the crucial role of fluctuations in pores with nanometric size. This is the typical scale of biological pore: it is then interesting to point out that biological pores are working at the edge of second law violation ($\bar{Q}_\tau \sim k_B T$).

These questions would deserve further experimental and theoretical investigations.

VI. DISCUSSION AND PERSPECTIVES

In this review, we hope to have convincingly shown that nanoscales do indeed play a key role in fluidics. A broad panel of length scales ranging from the molecular to the micrometric scales leads to a rich ensemble of nanofluidic phenomena. While the domain of validity of Navier-Stokes equations was shown to extend down to the nanometer scale, specific transport phenomena show up due the complex couplings which build up between flow and ionic transport, electrostatics, surface dynamics, etc.

We focused in this review on the behavior of fluids at the nanoscale. But in doing so we omitted several important topics in the discussions, however strongly connected to nanofluidics questions.

This concern in particular the field of transport of (macro)molecules, polymers, polyelectrolytes or biological molecules (DNA, RNA) through nanopores. This involves either biological nanopores, like the widely studied α -haemolysin, or artificial solid-state nanopores made by ionic drilling of membranes [139]. Starting from the pioneering work by Bezrukov *et al.* and Kasianowicz *et al.* [50, 51, 52], there has been a thorough exploration of the translocation mechanisms of macromolecules in tiny pores [140, 141], with important implications for the understanding of biological translocation process and potentially for single molecule analysis. This domain is now rapidly expanding and we refer to the recent review by C. Dekker for further reading [139].

Another aspect that we left aside is the question of nano- and micro- structured surfaces, in line with the recently developed super-hydrophobic surfaces exhibiting the Lotus effect. Superhydrophobic coatings can lead to huge slippage effects, with slip lengths in the micrometer range [46, 47, 142, 143], as well as other dynamic phenomena, such as hydro-elastic couplings at the super-

hydrophobic interface [144]. Such surfaces offer the possibility to considerably enhance the efficiency of transport phenomena in particular in the context of slip enhancement discussed above. For example, as we pointed out in the text, a massive amplification, by a factor up to 10^4 (!), is predicted for diffusio-osmosis on superhydrophobic surfaces, which offers the possibility to device efficient salt pumps [112]. The underlying coupling mechanisms remain however subtle, and this enhancement was shown for example to break down for electro-osmotic transport [112, 145]. The implications of nano- and micro- structuration on fluidic transport is still at its infancy and remains to be thoroughly explored. It offers the possibility to couple fluid dynamics over the scales, from the nano- to the micro-scales, and even to larger macroscopic scales [146].

Furthermore, beyond these questions, it is interesting to note that nanofluidics offer the possibility to attack old questions with new point of views, and new control possibilities. We quoted the amazing flow permeability measured by carbon nanotube membranes. While this performance remains to be understood – and possibly investigated at the individual nanotube level –, this opens very promising application in the field of energy, in particular for portable energy sources. Such membranes indeed offers the possibility of a very efficient conversion of hydrostatic energy to electrical power at small scales [102, 103], see also [147]. As we have discussed above, low (nanoscale) friction at surfaces considerably amplifies electrokinetic processes, such as electro-osmosis or streaming currents [98, 101]. The latter phenomenon is able to produce an electrical current from a pressure drop [148, 149]. On this basis it was argued [102, 103] that the efficiency of this mechano-electric transduction raises considerably for slippery walls : reasonable values suggest an increase of the energy conversion efficiency from a few percents to 30% for slippery surfaces ! While the tremendous effect of low surface friction and slippage on charge transport has been recently confirmed experimentally [101], its expected impact on mechano-electric energy conversion has not received an experimental confirmation. Extrapolating with the results obtained with the nanotube membranes, this power conversion efficiency raises to close to 100% (due to the expected extremely weak dissipation) and this amazing prediction would lead to a production of electrical power of several kW/m² for a pressure drop of 1bar [102]: this is an impressive result, which has not been confirmed up to now. While such predictions have to be taken with care, they strongly suggest to explore the role of nanofluidics in the context of energy conversion. Such nanofluidic energy conversion devices have a priori the potential to power larger scale systems (for example in cars or portable devices), due to their high power density and low weight [1].

An alternative field of application for the progress made in nanofluidic transport is desalination. Indeed, as half of the humanity has no immediate access to potable

water, desalination of seawater has emerged over the recent years as an alternative solution to develop fresh water. Reverse osmosis is one of the techniques used in this context, for example in the Ashkelon plant in Israel [150]: seawater is pushed through a membrane impermeable to the salt. Such a process is expensive (typically around 0.5\$/m³ for the Ashkelon plant in Israel [150]), due – among other factors – to the energy required to this operation. The possibility of reducing this energy by using a considerably more permeable membrane should have therefore a direct impact on the cost of produced water. This is a potential application of membranes made of carbon nanotubes which, as we discussed [9, 35, 36], exhibit a permeability 2 to 3 orders of magnitude higher than those with micropores, a fully unexpected and still debated result. Another question for the desalinated water is the mineral composition of the produced water which – if not controlled – could have a deep, negative, impact on agriculture and health. For example the concentration of Boron (B), which is toxic to many crops, is high in seawater, and requires to be partially eliminated by de-

salination post-treatments [150]. Reversely, desalination removes some ions which are essential to plant growth, such as Mg²⁺ or SO₄²⁻. There is therefore a potential need for a better selectivity of filtration.

Achieving selectivity similar to biological channels, such as aquaporins [8, 11, 12], is still out of reach, but nanofluidics has a major role to play in this context in order to find the key tuning parameters and architecture. Such applications may still be years away, but the basic principles underlying their operation will develop in the years to come.

Acknowledgments

We thank A. Ajdari, L. Auvray, C. Barentin, J.-L. Barrat, C. Cottin-Bizonne, R. Netz, D. Stein, and C. Ybert for many stimulating discussions. LB thank in particular D. Stein for illuminating discussions on the conductance effects.

-
- [1] Eijkel, J.C.T. and A. van den Berg, *Microfluidics and Nanofluidics*, 2005, **1**, 249-267
 - [2] A. Plecis, R.B. Schoch, and P. Renaud, *Nano Letters*, 2005, **5**, 1147-1155
 - [3] Q. Pu, J. Yun, H. Temkin, S. Liu, *NanoLetters*, 2004, **4** 1099
 - [4] R. B. M. Schasfoort, S. Schlautmann, J. Hendrikse, A. van den Berg, *Science*, 1999, **286**, 942
 - [5] R. Karnik, R. Fan, M. Yue, D. Li, P. Yang, and A. Majumdar, *NanoLetters*, 2005 **5** 943-948
 - [6] R. Karnik, C. Duan, K. Castelino, H. Daiguji, A. Majumdar, *Nano Letters*, 2007, **7** 547
 - [7] Z. Siwy, A. Fulinski, *Phys. Rev. Lett.*, 2002, **89**, 198103
 - [8] H. Sui, B.G. Han, J.K. Lee, P. Walian, B.K. Jap, *Nature*, 2001, **414** 872
 - [9] Holt, J. K., H. G. Park, Y. Wang, M. Stadermann, A. B. Artyukhin, C. P. Grigoropoulos, A. Noy, and O. Bakajin, *Science*, 2006, **312**, 1034
 - [10] K. Murata *et al.* *Nature*, 2000, **407** 599
 - [11] T. Walz, B.L. Smith, M.L. Zeidel, A. Engel, P. Agre, *J. Biol. Chem.*, 1994, **269** 1583
 - [12] M. Borgnia and P. Agre, *Proc. Natl. Acad. Sci. USA*, 2001, **98** 2888
 - [13] D. Y. C. Chan and R. G. Horn, *J. Chem. Phys.*, 1985, **83**, 5311
 - [14] J.-M. Georges, S. Millot, J.-L. Loubet and A. Tonck, *J. Chem. Phys.*, 1993, **98**, 7345.
 - [15] U. Raviv and J. Klein, *Science*, 2002, **297**, 1540
 - [16] T.-D. Li, J. Gao, R. Szożkiewicz, U. Landman, and E. Riedo, *Phys. Rev. B*, 2007, **75**, 115415
 - [17] A. Maali, T. Cohen-Bouhacina, G. Couturier, and J.-P. Aimé, *Phys. Rev. Lett.*, 2006, **96**, 086105
 - [18] T. Becker and F. Mugele, *Phys. Rev. Lett.*, 2003, **91**, 166104
 - [19] J. A. Thomas and A. J. H. McGaughey, *Phys. Rev. Lett.*, 2009, **102**, 184502
 - [20] Y. Leng, P.T. Cummings, *Phys. Rev. Lett.*, 2005, **94**, 026101
 - [21] L. Bocquet and J.-L. Barrat, *Soft Matter*, 2007, **3** 685
 - [22] L. Joly, C. Ybert, L. Bocquet, *Phys. Rev. Lett.*, 2006, **96**, 046101
 - [23] A. Saugey, L. Joly, C. Ybert, J.L. Barrat, and L. Bocquet, *J. Phys. Cond. Matt.*, 2005, **17**, S4075-S4090
 - [24] J. A. Thomas, and A. J. H. McGaughey, *Nano Letters*, 2008, **8**, 2788-2793
 - [25] Microscopic Derivation of Non-Markovian Thermalization of a Brownian particle, L. Bocquet, J. Piasecki, *J. Stat. Phys.*, 1997, **87** 1005
 - [26] E. Helfand, *Physical Review*, 1960, **119** 1
 - [27] S. Merabia, S. Shenogin, L. Joly, P. Keblinski, J.-L. Barrat, *Proc. Nat. Acad. SciUSA*, 2009, doi: 10.1073/pnas.0901372106
 - [28] G. Hummer, J.C. Rasalah, J.P. Noworyta, *Nature*, 2001, **414** 188
 - [29] T. Chou, *Phys. Rev. Lett.*, 1998, **80**, 85-88
 - [30] T. Chou and D. Lohse, *Phys. Rev. Lett.*, 1999, **82**, 3552-3555
 - [31] J.S. Hansen, P. J. Daivis, K. P. Travis, B.D. Todd *Phys. Rev. E*, 2007, **76**, 041121
 - [32] J. Goyon, A. Colin, G. Ovarlez, A. Ajdari, L. Bocquet, *Nature*, 2008, **454**, 84-87
 - [33] J.C. Rasaiah, S. Garde, G. Hummer, *Annual Review Physical Chemistry*, 2008, **59**, 713-740
 - [34] D. G. Levitt, *Phys. Rev. A*, 1973, **8** 3050
 - [35] M. Majumder *et al.*, *Nature*, 2005, **438** 44
 - [36] M. Whitby, L. Cagnon, M. Thanou, N. Quirke, *Nano Letters*, 2008, **8**, 2632
 - [37] S. Joseph and N. R. Aluru, *NanoLetters*, 2008, **8** (2), 452-458
 - [38] J. Israelachvili and H. Wennerström *Nature*, 1996, **379**, 219-225
 - [39] D. Andelman, in *Handbook of Biological Physics*, Vol-

- ume 1, edited by R. Lipowsky and E. Sackmann, Elsevier Science B.V., 1995.
- [40] Schoch, R.B., Han, J. and Renaud, P., *Reviews of Modern Physics*, 2008, **80**, 839-883
- [41] D. Stein, M. Kruithof, C. Dekker, *Phys. Rev. Lett.*, 2004, **93**, 035901
- [42] R. J. Hunter, *Foundations of colloid Science*, Oxford, 2nd Edition, 2001.
- [43] A. S. Khair, T. M. Squires, *J. Fluid. Mech.*, 2008, **615** 323-334.
- [44] R. Karnik, K. Castelino, R. Fan, P. Yang, and A. Majumdar, *NanoLetters*, 2005, **5** 1638-1642
- [45] D. Huang, C. Sendner, D. Horinek, R. Netz, L. Bocquet, *Phys. Rev. Lett.*, 2008, **101** 226101
- [46] P. Joseph, C. Cottin-Bizonne, J.-M. Benoît, C. Ybert, C. Journet, P. Tabeling, L. Bocquet, *Phys. Rev. Lett.*, 2006, **97**, 156104
- [47] C. Lee, C.-H. Choi, and C.-J. Kim, *Phys. Rev. Lett.*, 2008, **101**, 064501
- [48] Z. B. Ge, D. G. Cahill and P. V. Braun, *Phys. Rev. Lett.*, 2006, **96**, 186101.
- [49] P.-G. de Gennes, *Scaling Concepts in Polymer Physics*, Cornell University Press, Ithaca, 1979.
- [50] S. M. Bezrukov, I. Vodyanoy, V. A. Parsegian, *Nature*, 1993, **370** 279-281
- [51] S. M. Bezrukov, I. Vodyanoy, R. A. Brutyan, and J. J. Kasianowicz, *Macromolecules*, 1996, **29**, 8517-8522
- [52] J.J. Kasianowicz, E. Brandin, D. Branton, D.W. Deamer, *Proc. Natl. Acad. Sci. U.S.A.*, 1996, **93** 13770
- [53] Han, J. and H.G. Craighead, *Science*, 2000, **288**, 1026-1029
- [54] C. Navier, *Mem. Acad. Sci. Inst. Fr.*, 1823, **6**, 389-416
- [55] E. Lauga, M. Brenner and H. Stone, in *Microfluidics: The No-Slip Boundary Condition*, ed. C. T. J. Foss and A. Yarin, Springer, New-York, 2005, vol. Handbook of Experimental Fluid Dynamics, ch. 15
- [56] C. Neto, D. Evans, E. Bonaccorso, H.-J. Butt and V. J. Craig, *Rep. Prog. Phys.*, 2005, **68**, 2859-2897
- [57] P. Thompson and M. Robbins, *Phys. Rev. A*, 1990, **41**, 6830
- [58] L. Bocquet and J.-L. Barrat, *Phys. Rev. Letter*, 1993, **70**, 2726-2729
- [59] J.-L. Barrat and L. Bocquet, *Phys. Rev. E*, 1994, **49**, 3079-3092
- [60] M. Cieplak, J. Koplik and J. Banavar, *Phys. Rev. Lett.*, 2001, **86**, 803
- [61] N. Priezjev and S. Troian, *Phys. Rev. Lett.*, 2004, **92**, 018302
- [62] J.-L. Barrat and L. Bocquet, *Faraday Discuss.*, 1999, **112**, 119.
- [63] C. Sendner, D. Horinek, L. Bocquet, R. Netz, *Langmuir*, 2009, in press
- [64] J. Israelachvili and G. Adams, *Nature*, 1976, **262**, 774-6
- [65] O. Vinogradova, *Langmuir*, 1995, **11**, 2213-2220
- [66] J. Israelachvili, *J. Colloid Interf. Sci.*, 1986, **110(1)**, 263
- [67] Y. Zhu, S. Granick, *Phys. Rev. Lett.*, 2001, **87**, 096105
- [68] A. Steinberger, C. C. Cottin-Bizonne, P. Kleimann, and E. Charlaix, *Phys. Rev. Lett.*, 2008, **100**, 134501
- [69] C. Cottin-Bizonne, B. Cross, A. Steinberger and E. Charlaix, *Phys. Rev. Lett.*, 2005, **94**, 056102
- [70] C. Cottin-Bizonne, A. Steinberger, B. Cross, O. Raccurt and E. Charlaix, *Langmuir*, 2008, **24**, 1165-1172
- [71] V. Craig, C. Neto and D. Williams, *Phys. Rev. Lett.*, 2001, **87**, 0545041-4
- [72] E. Bonaccorso, M. Kappl and H.-J. Butt, *Phys. Rev. Lett.*, 2002, **88**, 076103-4
- [73] C. D. F. Honig and W. A. Ducker, *Phys. Rev. Lett.*, 2007, **98**, 028305
- [74] C. L. Henry and V. J. Craig, 2009, submitted to *Langmuir*
- [75] O. Vinogradova, H. Butt, G. Yabukov and F. Feuillebois, *Rev. Sci. Instrum.*, 2001, **72**, 2330
- [76] A. Maali, C. Hurth, T. Cohen-Bouhacina, G. Couturier and J.-P. Aimé, *Appl. Phys. Lett.*, 2006, **88**, 163504
- [77] A. Maali, T. Cohen-Bouhacina and H. Kellay, *Appl. Phys. Lett.*, 2008, **92**, 053101
- [78] D. Tretheway, C. Meinhart, *Phys. Fluids*, 2002, **14(3)**, L9-L12
- [79] D. Lumma, A. Best, A. Gansen, F. Feuillebois, J. Radler and O.I. Vinogradova, *Phys. Rev. E*, 2003, **67**, 056313
- [80] P. Joseph and P. Tabeling, *Phys. Rev. E*, 2005, **71**, 035303
- [81] O.I. Vinogradova, K. Koynov, A. Best, F. Feuillebois, *Phys. Rev. Lett.*, 2009, **102**, 118302
- [82] D. Lasne, A. Maali, Y. Amarouchene, L. Cognet, B. Lounis, and H. Kellay, *Phys. Rev. Lett.*, 2008, **100**, 214502
- [83] W.A. Ducker, *Langmuir*, 2009, **25**, 8907-8910
- [84] B. Borkent, S. Dammer, H. Schonherr, G. Vancso and D. Lohse, *Phys. Rev. Lett.*, 2007, **98**, 204502
- [85] S. Yang, S. Dammer, N. Bremond, E. Zandvliet, H.J.W. Kooij and D. Lohse, *Langmuir*, 2007, **23**, 7072-7077
- [86] T. Becker and F. Mugele, *Phys. Rev. Lett.*, 2003, **91(16)**, 166104
- [87] R. Pit, H. Hervet and L. Léger, *Phys. Rev. Lett.*, 2000, **85**, 980-983
- [88] T. Schmadtko, H. Hervet and L. Leger, *Phys. Rev. Lett.*, 2005, **94**, 244501
- [89] J. L. Anderson, *Annu. Rev. Fluid Mech.*, 1989, **21**, 61
- [90] Y. Levin, E. Trizac, L. Bocquet, *J. Phys. Cond. Matter*, 2003, **15** S3523-S3536
- [91] I. Rouzina and V.A. Bloomfield, *J. Phys. Chem*, 1996, **100**, 9977-9989.
- [92] D. M. Huang, C. Cottin-Bizonne, C. Ybert, L. Bocquet, *Langmuir*, 2008, **24** 1442-1450
- [93] W. Kunz, J. Henle, and B.W. Ninham, *Curr. Opin. Colloid Interface Sci.*, 2004, **9**, 19
- [94] D. Horinek and R. Netz, *Phys. Rev. Lett.*, 2007, **99** 226104
- [95] P. Jungwirth and D. J. Tobias, *Chem. Rev.*, 2006, **106**, 1259-1281
- [96] D. M. Huang, C. Cottin-Bizonne, C. Ybert, L. Bocquet, *Phys. Rev. Lett.*, 2007, **98**, 177801
- [97] V. Buch *et al.*, *Proc. Nat. Acad. Sci. USA*, 2007, **104**, 7342
- [98] L. Joly, C. Ybert, E. Trizac, L. Bocquet, *Phys. Rev. Lett.*, 2004, **93**, 257805
- [99] V. M. Muller *et al.*, *Colloid J. USSR*, 1986, **48**, 718
- [100] N. V. Churaev, J. Ralston, I. P. Sergeeva, and V. D. Sobolev, *Adv. Colloid Interface Sci.*, 2002, **96**, 265
- [101] C. I. Bouzigues, P. Tabeling, and L. Bocquet, *Phys. Rev. Lett.*, 2008, **101**, 114503
- [102] Y. Ren and D. Stein, *Nanotechnology*, 2008, **19**, 195707
- [103] S. Pennathur, E. Eijkel, A. Ven der Berg, *Lab on a Chip*, 2007, **7** 1234
- [104] R. Qiao and N. R. Aluru, *Phys. Rev. Lett.*, 2004, **92**

- 198301
- [105] D. Horinek, A. Herz, L. Vrbka, F. Sedlmeier, S.I. Matkukulov, R. R. Netz, submitted to *J. Am. Chem. Soc.*, 2009
- [106] R. Piazza, *Soft Matter*, 2008, 4, 1740-1744
- [107] S. Duhr, D. Braun, *Proc. Natl. Acad. Sci. USA*, 2006, **103** 19678- 19682
- [108] H.-R. Jiang, H. Wada, N. Yoshinaga, and M. Sano, *Phys. Rev. Lett.*, 2009, **102**, 208301
- [109] A. Wurger, *Phys. Rev. Lett.*, 2008, **101**, 108302
- [110] J.P. Ebel, J.L. Anderson, and D.C. Prieve *Langmuir*, 1988, **4**, 396 - 406
- [111] B. Abécassis, C. Cottin-Bizonne, C. Ybert, A. Ajdari, L. Bocquet, *Nature Materials*, 2008, **7** 785
- [112] D. M. Huang, C. Cottin-Bizonne, C. Ybert, L. Bocquet, *Phys. Rev. Lett.*, 2008, **101**, 064503
- [113] Armand Ajdari, L. Bocquet, *Phys. Rev. Lett.*, 2006, **96** 186102
- [114] J. Morthomas and A. Wurger, *J. Phys. Cond. Matt.*, 2009, **21** 035103
- [115] C. Ybert, C. Barentin, C. Cottin-Bizonne, P. Joseph, L. Bocquet, *Phys. Fluids*, 2007, 19, 123601
- [116] S. Levine, J.R. Marriott, K. Robinson, *J. Chem. Soc. Faraday Trans. II*, 1975, **711**-11
- [117] H. Daiguji, P. Yang, A. Majumdar, *Nano Letters*, 2004, **4** 137-142
- [118] C. Dellago, M.N. Naor, G. Hummer, *Phys. Rev. Lett.*, 2003, **90** 105902.
- [119] S. R. De Groot and P. Mazur, *Non-Equilibrium Thermodynamics*, North-Holland, Amsterdam, 1969.
- [120] E. Brunet and A. Ajdari, *Phys. Rev. E*, 2004, **69**, 016306
- [121] O. Kedem and A. Katchalsky, *J. Gen. Physiol.*, 1961, **45** 143
- [122] O. Kedem and A. Katchalsky, *Trans. Faraday Soc.*, 1963, **59** 1941-1953
- [123] Y.C. Wang, A. L. Stevens, J. Han, *Anal. Chem.*, 2005, **77** 4293-4299
- [124] A. Plecis, C. Nanteuil, A.-M. Haghiri-Gosnet, and Y. Chen, *Analytical Chemistry*, 2009, **80** 9542-9550
- [125] C. Kittel, *Introduction to Solid State Physics*, Wiley, 5th Edition, 1976
- [126] Z. Siwy, I.D. Kosińska, A. Fuliński, C.R. Martin, *Phys. Rev. Lett.*, 2005, **94**, 048102
- [127] R.M.M. Smeets, U.F. Keyser, N.H. Dekker, C. Dekker, *Proc. Natl. Acad. Sci. U.S.A.*, 2008, **105** 417-421
- [128] A. Kalra, S. Garde, and G. Hummer, *Proc. Natl. Acad. Sci. USA*, 2003, **100**, 10175
- [129] A. Berezhkovskii and G. Hummer, *Phys. Rev. Lett.*, 2002, **89**, 064503
- [130] M. Moseler and U. Landman, *Science*, 2000, **289**, 1165
- [131] B. Davidovitch, E. Moro and H.A. Stone, *Phys. Rev. Lett.*, 2005, **95**, 244505
- [132] G. Grün, K. Mecke, and M. Rauscher, *J. Stat. Phys.*, 2006, **122**, 1261
- [133] J. Becker, G. Grün, R. Seemann, H. Mantz, K. Jacobs, K. R. Mecke and R. Blossey, *Nature Materials*, 2003, **2**, 59
- [134] L. D. Landau and E. M. Lifshitz, *Statistical Physics*, Pergamon Press, London, 1958.
- [135] F. Ritort, *J. Phys. Condens. Matter*, 2006, **18**, R531
- [136] D. J. Evans, E.G.D. Cohen, G.P. Morriss, *Phys. Rev. Lett.*, 1993, **71** 2401-2404
- [137] R. van Zon and E.G.D. Cohen, *Phys. Rev. Lett.*, 2003, **91** 110601
- [138] R. van Zon, S. Ciliberto, and E. G. D. Cohen *Phys. Rev. Lett.*, 2004, **92** 130601
- [139] C. Dekker, *Nature Nanotech.*, 2007, **2**, 209-215
- [140] G. Oukhaled, J. Mathe, A.-L. Biance, *et al. Phys. Rev. Lett.*, 2007, **98**, 158101
- [141] S. van Dorp, U. F. Keyser, N. H. Dekker, C. Dekker and S. G. Lemay, *Nature Physics*, 2009, **5**, 347 - 351
- [142] C. Cottin-Bizonne, J.-L. Barrat, L. Bocquet, E. Charlaix, *Nature Materials*, 2003, **2** 238
- [143] J. Ou and J. P. Rothstein, *Phys. Fluids*, 2005, **17**, 103606
- [144] A. Steinberger, C. Cottin-Bizonne, P. Kleimann, E. Charlaix, *Nature Materials*, 2007, **6**, 665
- [145] T. Squires, *Phys. Fluids*, 2008, **20**, 092105
- [146] C. Duez, C. Ybert, C. Clanet, L. Bocquet, *Nature Physics*, 2007, **3**, 180-183
- [147] Y. Zhao *et al.* , *Adv. Materials* , 2008, **20**, 1772
- [148] F.H.J. van der Heyden, D.J. Bonthuis, D. Stein, C. Meyer, and C. Dekker, *Nano Letters*, 2006, **6**, 2232 - 2237
- [149] F.H.J. van der Heyden, D.J. Bonthuis, D. Stein, C. Meyer, and C. Dekker, *Nano Letters*, 2007, **7**, 1022-1025
- [150] U. Yermiyahu *et al.* , *Science*, 2007, **318**, 920
- [151] “Par ma foi ! il y a plus de quarante ans que je dis de la prose sans que j’en susse rien, et je vous suis le plus obligé du monde de m’avoir appris cela.”, which translates into “By my faith! For more than forty years I have been speaking prose without knowing anything about it, and I am much obliged to you for having taught me that.”
- [152] We specifically thank D. Stein for very interesting discussions concerning this point.
- [153] We choose here to define the zeta potential as the one appearing in the Smoluchowski formula. According to Eq.20, this may differ from the surface potential, depending on conditions. Another possibility would have been to define the zeta potential as V_0 and consider an amplified zeta potential. We preferred to use the former definition.